



Calhoun: The NPS Institutional Archive
DSpace Repository

Theses and Dissertations

1. Thesis and Dissertation Collection, all items

1993

Design and construction of an experimental
filament winding machine.

Lutkenhouse, Mark Geoffry.

<http://hdl.handle.net/10945/24145>

Downloaded from NPS Archive: Calhoun



Calhoun is the Naval Postgraduate School's public access digital repository for research materials and institutional publications created by the NPS community. Calhoun is named for Professor of Mathematics Guy K. Calhoun, NPS's first appointed -- and published -- scholarly author.

Dudley Knox Library / Naval Postgraduate School
411 Dyer Road / 1 University Circle
Monterey, California USA 93943

<http://www.nps.edu/library>

DUDLEY KNOX LIBRARY
NAVAL POSTGRADUATE SCHOOL
MONTEREY CA 93943-5101

DESIGN AND CONSTRUCTION OF AN EXPERIMENTAL
FILAMENT WINDING MACHINE

T260689

DESIGN AND CONSTRUCTION OF AN EXPERIMENTAL
FILAMENT WINDING MACHINE

by

MARK GEOFFRY LUTKENHOUSE, B.S.

THESIS

Presented to the Faculty of the Graduate School of

The University of Texas at Austin

in Partial Fulfillment

of the Requirements

for the Degree of

MASTER OF SCIENCE IN ENGINEERING

THE UNIVERSITY OF TEXAS AT AUSTIN

May 1993

ACKNOWLEDGMENTS

This research, like most successful ventures, was possible through the contributions and input of many talented individuals. I would like to give a special thanks to the following (listed in alphabetical order):

Bih-Cherng Chern who provided insights into methods to approach the construction and testing of the project and rendered significant assistance in solving analytical problems.

Chin Seng Chu and Wiling Tan who provided significant assistance in the computer setup, software programming and various hardware connections.

Elvin Estes for his instruction in the operation of a filament winding machine.

Hank Franklin and his department of machinists and electrical technicians whose knowledge and vast experience led to the overall construction of the machine and practical solutions to numerous engineering problems.

Dr. John Howell whose vast knowledge of Heat Transfer is surpassed only by his patience and ability to educate others in a very tough and theoretically demanding field.

Dr. Tess Moon whose motivation and inspiration brings out the best in those fortunate enough to work for her.

Steve Orwick who provided invaluable advice and supervision in the setup and testing of the project.

Jason Weis who spent many hours verifying calculations and analytical approaches, machining, and troubleshooting the project.

Finally, I would like to give a very special thanks to:

The One and only God. Through Him all things are possible.

My wife for her strategic and tactical assistance and advice during the whole operation of completing the graduate program and for being a steady hand and guiding light.

The United States Navy Civil Engineer Corps for the opportunity to advance my education.

"The nose of the bulldog is slanted backwards so he can continue to breathe without letting go." - Winston Churchill

This thesis is submitted to the Committee on 8 January, 1993.

TABLE OF CONTENTS

	Page
ACKNOWLEDGEMENTS	iv
LIST OF TABLES	viii
LIST OF FIGURES	ix
NOMENCLATURE	xi
Chapter	
1 INTRODUCTION	1
1.1 Conceptual Design	2
1.2 Construction Materials	5
2 THE FRAME	8
3 THE MANDREL AND CARRIAGE ASSEMBLY	13
3.1 Determining the Conductive Heat Loss	14
3.2 Dimensioning Specific Mandrel Parts	18
3.3 Calculating Potential Slip of the Filament Wrap	18
3.4 Strength Computation of the Disc Lip	20
3.5 Carriage Assembly	22
4 THERMOCOUPLE ASSEMBLY	25
5 THE HEAT SHIELD	34
6 MACHINING	37
7 THE MOTION CONTROL SYSTEM	46
8 EXPERIMENTATION AND RESULTS	51
APPENDIX A	57

	Page
APPENDIX B	64
APPENDIX C	69
APPENDIX D	75
APPENDIX E	80
APPENDIX F	87
APPENDIX G	89
APPENDIX H	99
APPENDIX I	106
APPENDIX J	110
APPENDIX K	111
APPENDIX L	113
REFERENCES	114

LIST OF TABLES

Table	Page
1.1 Material Specifications	6
1.2 Carbon Filament Specifications	7
7.1 Motion Control System Specifications	50
8.1 Prepreg Tape Cure Time vs Temperature	52

LIST OF FIGURES

Figure	Page
1.1 Filament Winding Machine (Three Dimensional View)	3
2.1 Frame (Three Dimensional View)	9
2.2 Frame (Plan View)	10
3.1 Mandrel (Three Dimensional View)	15
3.2 Mandrel (Scale)	16
3.3 Mandrel Tow Around Mandrel	19
3.4 Clamp (Top View and Section)	21
3.5 Carriage Assembly (Scale)	23
4.1 Thermocouple Acquisition System	26
4.2 Resistance in a Thermocouple Wire	29
4.3 Thermocouple Injection Assembly	31
5.1 Mandrel Positioned under the Lamp Bank	34
6.1 Bolt Characteristics	41
6.2 Bolt Diameter vs Depth of Hole	43
A.1 Mechanical Representation of Machine	57
A.2 Bond Graph Model of Machine	58
B.1 Mandrel and Heat Lamp Bank	64
B.2 Mandrel (Axial Section View)	66
C.1 Bolt Pattern (Inner Discs)	73
C.2 Bolt Pattern (Outer Discs)	74
D.1 Filament Wrapped Around the Mandrel	76

D.2 Force Summation of the Filament	77
E.1 Disc Lip	81
F.1 Thermocouple under Centrifugal Force	87
G.1 Heat Transfer Network from the Lamp Bank to the Outside Air	89
G.2 Lamp Bank, Shields, and Mandrel Assembly (End Section View)	90
G.3 Enclosure Geometry to Determine View Factor	91
G.4 Effective Light Emission on Lamp Bank	94
H.1 Defining Geometry for View Factor	99
H.2 Configuration of Mandrel to Heat Shield	102
H.3 Nusselt Geometric Analysis to Determine View Factor	104
H.4 Lamp Bank over Elemental Mandrel Area	105
J.1 Mandrel inside Oven	110
L.1 Filament Temperature Profile over Time	113

NOMENCLATURE

m	total mass of the mandrel, meters
m_e	eccentric mass of the mandrel during rotation
K	effective stiffness of the frame
b	effective resistance of the four shock absorbers and frame
P	total implied load of the mandrel
P_m	load of the mandrel due to its mass
P^O	reaction force
v_k	velocity of the frame (at the center of mass) due to vibrations
v_b	velocity of the dampers (at the center of mass) due to vibrations
v	velocity of the mandrel (at the center of mass)
p	momentum of the mandrel (at the center of mass)
ω	angular velocity of the mandrel
ω_n	natural frequency of the frame
η	ω/ω_n = ratio of forced frequency to natural frequency
r	radius of m_e from the longitudinal axis of the mandrel
x	displacement of the frame (at the center of mass)
B	amplitude of the frame's displacement
ϕ	phase difference between the input force and the displacement of the frame
R_i	thermal resistance of the blanket insulation
R_r	thermal resistance of the refractory material
R_s	thermal resistance of the steel cylinder

T_{in}	temperature of the filament tape nearest to the steel mandrel
T_{out}	average temperature of the steel shaft in contact with the insulation
T_1	effective temperature of the heat lamp bank
T''	temperature of the filament tape nearest to the heat lamp bank
T_2	temperature of the heat shield
T_3	temperature of the heat shield
T_4	temperature of the steel cylinder in contact with the filament
T_{eff}	temperature of the effective lamp bank
T_{Bi}	temperature of the side of the heat shield facing the lamp bank
T_{Bo}	temperature of the side of the heat shield facing away from the lamp bank
q_{rad}	radiation heat flux from the lamp bank to the filament wound cylinder
q_{cond}	conductive heat loss of the mandrel
A_1	surface area of the lamp bank heat source
ε_1	emissivity of the heat lamp bank
A_{4t}	total surface area of the mandrel
ε_2	emissivity of carbon
F_{14}°	ideal view factor from the lamp bank to the mandrel with no loss
F_{14}	view factor from the lamp bank to the mandrel with shields connected to the system
r_s	radius of the steel shaft
r_i	inner radius of the steel cylinder
r_o	outer radius of the steel cylinder
k_s	thermal conductivity of steel

k_i	thermal conductivity of the blanket insulation
k_l	thermal conductivity of the lava rock
L	length
in	inches
J	joules
W	watts
lbf	pound force
cm	centimeters
Pa	Pascals
N	Newtons
θ	winding angle of the filament tape with respect to the mandrel
F	tension load of the filament tape as it winds onto the mandrel
F_f	frictional force between the filament and the mandrel
F_t	axial force imposed on the filament by the mandrel
μ	frictional coefficient
μ_{cs}	frictional coefficient between steel and carbon
μ_{cc}	frictional coefficient between carbon and carbon
δ_s	deformation of the shaft (radius) due to thermal expansion
ν	Poisson's ratio
ν_s	Poisson's ratio of steel
r_{is}	inner radius of the steel shaft
r_{os}	outer radius of the steel shaft
δ_l	deformation of the lava disc (inner radius) due to thermal expansion
ν_l	Poisson's ratio of the lava disc

r_{il}	inner radius of the lava disc
r_{ol}	outer radius of the lava disc
δ_{tot}	total interference between the shaft and lava disc due to a press fit
ε	linear strain
σ_r	radial stress
σ_{rs}	radial stress of the steel shaft
σ_{rl}	radial stress of the lava disc
σ_{θ}	tangential stress
$\sigma_{\theta s}$	tangential stress of the steel shaft
$\sigma_{\theta l}$	tangential stress of the lava disc
ε_r	radial strain
ε_{rs}	radial strain of the steel shaft
ε_{rl}	radial strain of the lava disc
ε_{θ}	tangential strain
$\varepsilon_{\theta s}$	tangential strain of the steel shaft
$\varepsilon_{\theta l}$	tangential strain of the lava disc
α	linear coefficient of thermal expansion
E	modulus of elasticity
E_s	modulus of elasticity (steel)
E_c	modulus of elasticity (copper)
E_A	modulus of elasticity (aluminum)
E_l	modulus of elasticity (lava rock)
ΔT	temperature change on the discs and mandrel due to activation of oven
p_r	axisymmetric pressure

σ_x	stress on the lip (x-direction)
σ_y	stress on the lip (y-direction)
τ_{xy}	shear stress on the lip
\bar{F}	uniform load per unit length and width imposed on the lip by the clamp
g	one half the thickness of the lip
J_t	mass moment of inertia for the thermocouple about its longitudinal axis
\bar{w}	centrifugal force per length of the thermocouple
d	thermocouple wire diameter, depth of lip
ρ	density of the thermocouple
a	radial acceleration of the thermocouple due to the mandrel's rotational velocity
I_x	moment of inertia of thermocouple
r_t	distance of thermocouple to the center of the mandrel
\bar{R}_s	resistance of copper wire in thermocouple
\bar{R}_L	resistance of the thermocouple wire coating
σ	Stefan-Boltzmann constant = $5.6697 \times 10^{-8} \text{ W/m}^2 \text{ K}^4$
ρ_j	reflectivity of side j
α_j	absorbtivity of side j
ε_j	emissivity of side j
q_i^-	heat flux being absorbed by side i
q_i^+	heat flux being radiated by side j
F_{ij}	view factor between sides i and j
n	number of sides
δ_{ij}	delta function

A_i	area of side i , area of elemental surface i
A_t	circumferential area of individual lamp in lamp bank
r_t	lamp radius
l_t	lamp length
n_t	number of tubes in the lamp bank
T_{eff}	effective temperature of the lamp bank
ε_{eff}	effective emissivity of the lamp bank
T_i	temperature of individual lamp in the lamp bank
w_l	convective heat transfer coefficient
N_u	Nusselt number
R_e	Reynolds number
Pr	Prandtl number
L_l	effective shield length
k_a	thermal conductivity of air
ν_a	kinematic viscosity of air
g	gravity
β	volume expansive coefficient
$\Delta\rho/\rho$	density change of air due to thermal change
ν_k	kinematic viscosity
S	finite surface area
a	angle between normal of elemental surface dA_1 and imaginary line to surface dA_2
b	angle between normal of elemental surface dA_2 and imaginary line to surface dA_1

S	distance between dA_1 and dA_2
ω_i	angular velocity of object i
T_i	torque of object i
d_m	mandrel diameter
v_{mo}	linear velocity of mandrel taken at outside diameter
t_f	tension of filament as it is being wound onto the mandrel
m_1	motor 1
m_2	motor2
T_{ai}	torque on object i due to acceleration
t	time
J_i	mass moment of inertia of object i
J_s	mass moment of inertia of mandrel shaft
J_{id}	mass moment of inertia of inner disc
J_{sc}	mass moment of inertia of steel cylinder
J_{isd}	mass moment of inertia of inner steel donut
J_{osd}	mass moment of inertia of outer steel donut
J_{od}	mass moment of inertia of outer disc
r_{ii}	inner radius of object i
r_{oi}	outer radius of object i
ρ_i	density of object i
l_i	length of object i
g_c	gravitational constant = $100 \text{ cm kg/sec}^2 \text{ N}$
α_m	angular acceleration of mandrel
$\eta_c p_c$	efficiency of the carriage assembly

v_c	carriage velocity
w_c	weight of carriage assembly
p_c	screw pitch of carriage assembly
R	screw radius
L_s	length of screw
ρ_s	screw density
J_s	mass moment of inertia of the lead screw
J_c	mass moment of inertia of the carriage assembly
ID	inner diameter
OD	outer diameter
z	disc slot length
δ	deformation of lip per unit length
I_l	moment of inertia of lip
h	width of lip
$R_{rad\ eff}$	effective thermal resistance due to radiation in closed system
R_{cond}	thermal resistance due to conduction
R_{rad}	thermal resistance due to radiation
R_{conv}	thermal resistance due to convection

1 INTRODUCTION

Current research programs in composite manufacturing underway in the Mechanical Engineering Department of the University of Texas at Austin have led to the need to acquire a machine capable of filament winding composites under experimental conditions. Purchase of a standard filament winding machine could not satisfy this requirement as it would be too big and require refitting for thermal analysis. Consequently, the decision was made to design and construct a machine capable of fitting inside an existing infrared (IR) oven thus allowing control of the heat transfer process.

The design and construction of the filament winding machine was conducted under prescribed requirements and conditions. The resulting machine had to support the current studies in composite manufacturing and obviously be compatible with existing products on the market. The machine had to utilize carbon filament of different sizes, and produce cylinders of different lengths and winding patterns.

The design was kept simple and straightforward to limit complexity, minimize development costs, and reduce construction time. The filament winder employed an existing rail table, off the shelf solenoids and thermocouples, standard motion control systems, and was constructed with readily available materials, thereby ensuring short lead times. The design specifications were calculated conservatively whenever possible to ensure both reliability and

durability of the finished product. This thesis details the processes and procedures used in the design, construction, and testing of a filament winding machine.

1.1 CONCEPTUAL DESIGN

The author initiated only a conceptual design of the filament winding machine before beginning construction due to the short time available for its design and construction. The basic outline is modeled after the filament winding machine located in the Center for Electromechanics at Balcones Laboratory. The machine is designed to have two axle motion, a spinning mandrel and a carriage assembly. The carbon filament wraps around the mandrel as the carriage assembly guides it along the mandrel's longitudinal axis and determines the winding pattern (Figure 1.1). The design of the filament winder also had to satisfy the following requirements to ensure useability with ongoing research:

- (1) Limited overall dimensions allowing placement inside an existing infrared oven.
- (2) Ability to withstand and operate in a heated oven .
- (3) Insignificant heat transfer effect on the filament during the winding operation.
- (4) Capability to measure the filament temperature during the winding operation.

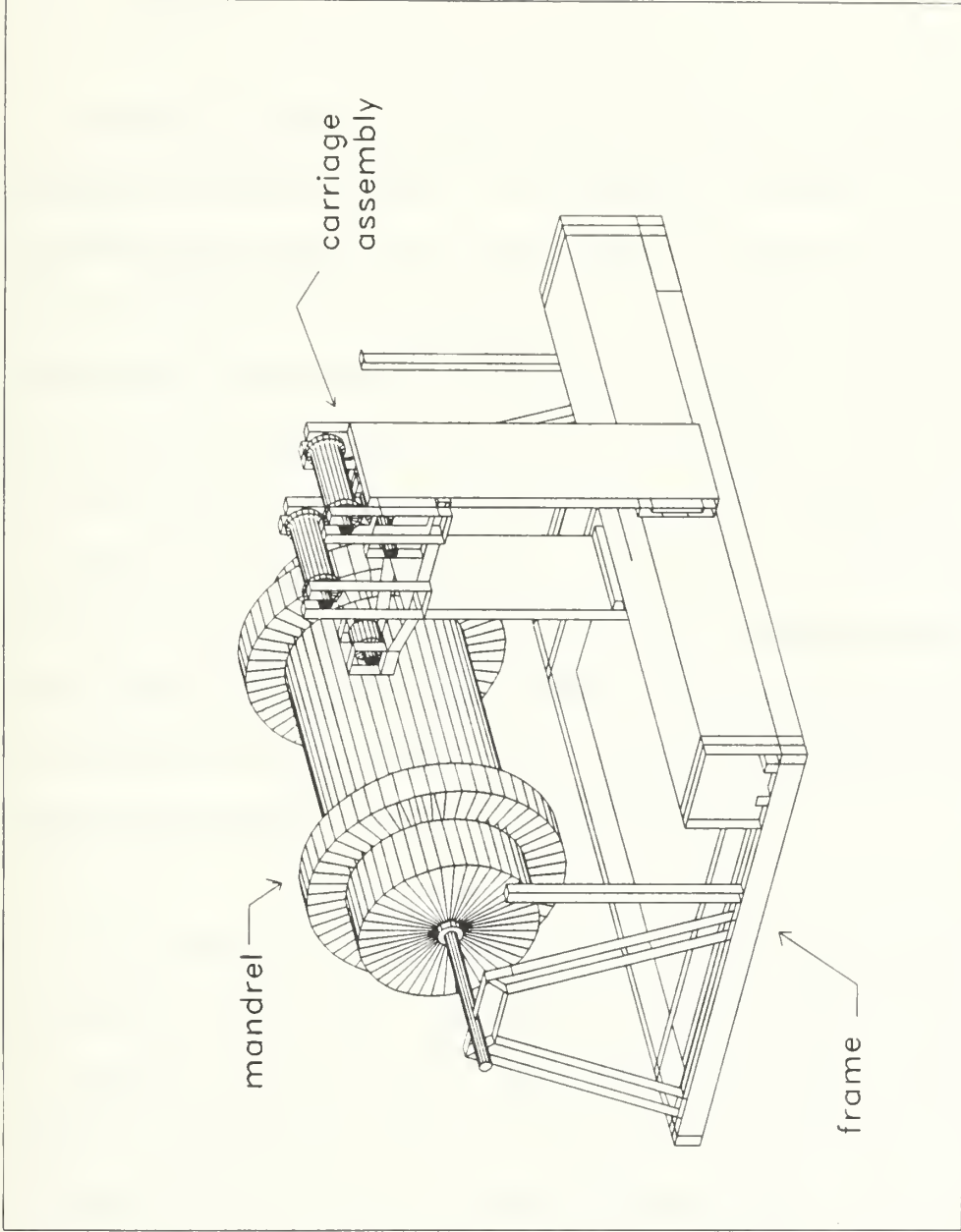


Figure 1.1: Filament Winding Machine (Three Dimensional View)

- (5) Maximum speed of twelve revolutions per second during the winding operation.

Initiating a conceptual design allowed the freedom to change and modify the apparatus during construction. This adaptability was essential since use of any available parts helped control project costs and speed construction. Once found, many parts required modification for the project or adaptation of the original filament winder design to incorporate the new part. Although the added flexibility was beneficial, this approach did have drawbacks. Parts occasionally had to be reworked or the design altered after a section was finished to meet a new part or a change in the function. Additionally, a complete analytical evaluation of the model could not be done. Stress and load calculations were done to determine if the concept was feasible, though a considerable amount of the construction was performed using conservative estimation due to the various unknown variables and boundary conditions.

The winding operation speed was forecasted at approximately 720 revolutions per minute (rpm). Considering the potential problems encountered with equipment rotating at such high speeds, extreme care was taken to minimize any eccentricity of the rotating parts. Most parts were manufactured with excess mass to reduce unavoidable vibration effects. All bearings and raceways were designed and built to exact tolerances to minimize slop and possible sources of vibration. This was a time consuming, but necessary process.

1.2 CONSTRUCTION MATERIALS

The machine was constructed primarily of steel and aluminum as these materials provide high melting temperatures, good structural characteristics and were readily available. Insulating materials consisted primarily of lava rock and Kaowool insulation. Material specifications of the construction materials are provided in Table 1.1.

The Hercules Company of Magna, Utah was the source of the primary composite material employed by the filament winder. The carbon filament prepreg is available from Hercules in various shapes and sizes. Prepreg tape is an amine-cured epoxy resin reinforced with unidirectional carbon fibers. The machine was designed around tape with widths ranging from 0.055 inches to 3 inches (1.4 cm to 7.6 cm). Initial testing dictated use of a prepreg "wrap" with a width of 3 inches (7.6 cm). This wrap was the basis of the design for the tensioning system. Specifications for the carbon filament are outlined in Table 1.2.

TABLE 1.1

MATERIAL SPECIFICATIONS

1. Carbon Steel (G10180)	
yield strength	32 kpsi (2.2 EE8 Pa)
tensile strength	58 kpsi (4.0 EE8 Pa)
modulus of elasticity	29 EE6 psi (2 EE11 Pa)
shear modulus	11.5 EE6 psi (8 EE11 Pa)
Poisson's ratio	0.30
density	489 pcf (7830 kg/m ³)
thermal heat constant	6.5 EE-6 1/F (3.6 EE-5 1/K)
2. Aluminum Alloy (A96061)	
yield strength	8 kpsi (5.5 EE7 Pa)
tensile strength	18 kpsi (1.2 EE8 Pa)
modulus of elasticity	10 EE6 psi (6.9 EE10 Pa)
shear modulus	3.9 EE6 psi (2.7 EE10 Pa)
Poisson's ratio	0.33
density	173 pcf (2770 kg/m ³)
thermal heat constant	12.8 EE-6 1/F (23 EE-6 1/K)
3. Lava (Grade "A" aluminum silicate)	
specific gravity	2.3
density	147 pci (2352 kg/m ³)
tensile strength	3 kpsi (2.1 EE7 Pa)
compressive strength	25 kpsi (1.7 EE8 Pa)
flexural strength	10 kpsi (6.9 EE7 Pa)
softening temperature	2912 (F) 1873 (C)
thermal heat constant	6.5 EE-6 1/F (11.7 EE-6 1/K)
thermal conductivity	3.5 Btu/hr ft F (6.1 J/sec m C)
Poisson's ratio	0.21
4. Kaowool Blanket Insulation	
temperature rating	2300° F (1260° C)
melting point	3200° F (1760° C)
continuous use limit	2000° F (1093° C)
density	6 pcf (96 kg/m ³)
thermal conductivity	0.5 Btu in/hr sf F (.865 J/sec m C)

TABLE 1.2

CARBON FILAMENT SPECIFICATIONS
(HERCULES CARBON PREPREG TAPE)

Typical Composite Properties

0° Tensile strength at 77° F	310 kpsi (2.1 EE9 Pa)
0° Tensile Modulus at 77° F	21.5 EE3 kpsi (1.5 EE8 Pa)
0° Compression strength at 77° F	240 kpsi (1.7 EE9 Pa)
Fiber volume	62%
Cured ply thickness	5.2 mils (.13 mm)

Typical Prepreg Characteristics

Fiber areal weight	4.4 oz/yd ² (150 g/m ²)
Standard width	12 in (30.5 cm)
Approximate yield	
at 42 % resin content	18.8 ft/lb (12.6 m/kg)
at 35 % resin content	21.2 ft/lb (14.2 m/kg)
Resin content, % by weight	42 \pm 3 %, 35 \pm 3 %
Gel time at 350° F	6-12 minutes
volatile content, % by weight	1 % max
Out time at room temperature	10 days min
Shelf life at 0° F	12 months

2 THE FRAME

The entire winding operation rests on a support consisting of a modified A-frame atop a rectangular frame (Figures 2.1 and 2.2). It is built of c-channel section of carbon steel. The c-channel provides good structural strength for the design and furnishes flat surfaces for welding and placement of equipment. The frame is welded for structural strength and its overall dimensions allow placement inside an existing infrared oven for testing. The initial design also included four rubber shock absorbers affixed to the frame at each of the four corners. This was an attempt to lower the transmissibility from the frame to the oven.

The actual in-service loads to be imposed on the frame were unknown at the time of construction. The steel section, therefore, was determined based on an estimate of the applied loads with the expectation of adding structural support if it became necessary. A bond graph model was developed to study the dynamics of the frame and loads that would be applied at specified transmission points. The primary motion was rotational and originated from the mandrel and the motor.

Figure A.1 in Appendix A shows a simplified mechanical representation of the filament winding machine. The mass represents the mandrel which contains a specified static force (weight) and a radial force (eccentricity). The spring represents the cumulative stiffness of the frame.

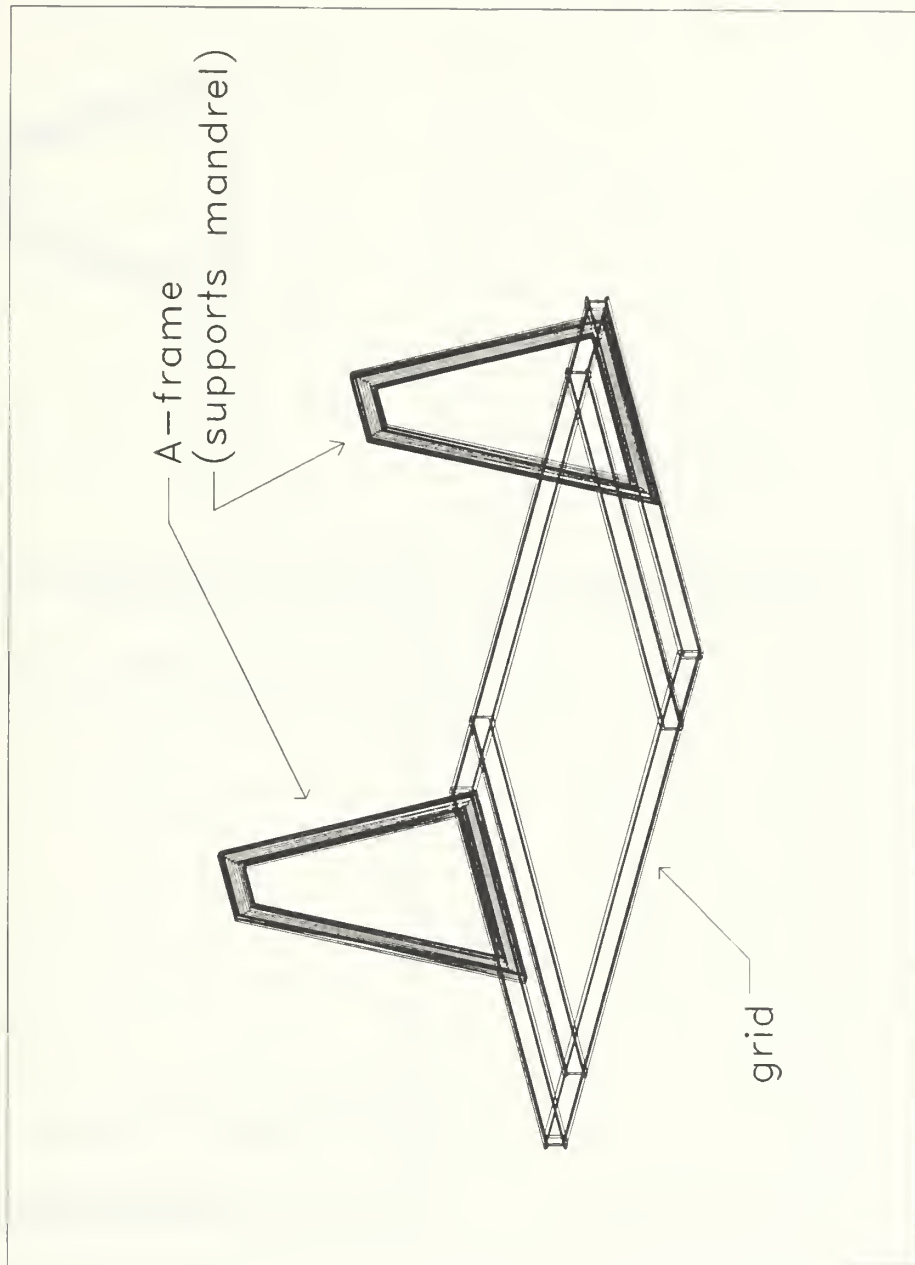


Figure 2.1: Frame (Three Dimensional View)

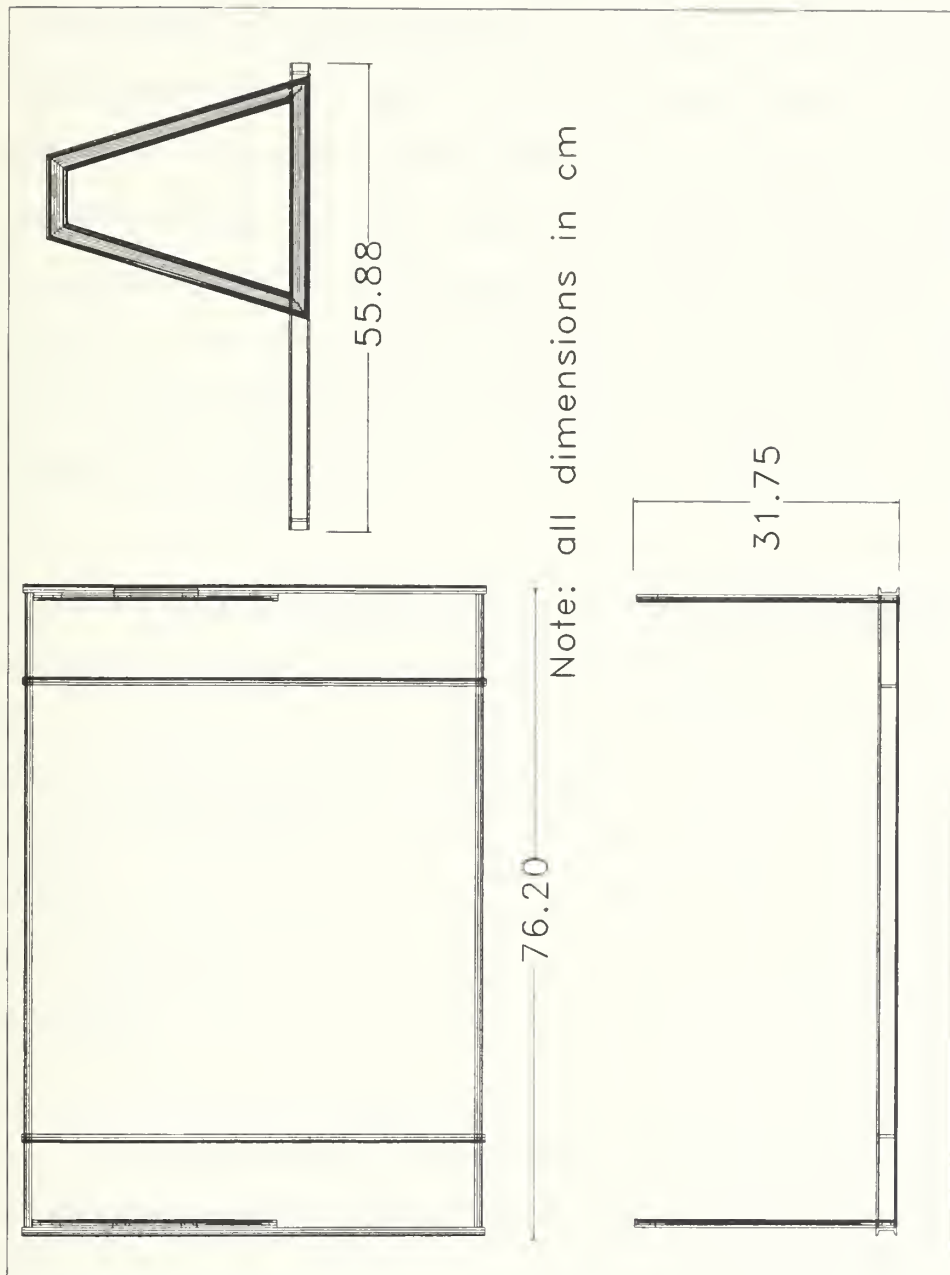


Figure 2.2: Frame (Plan View)

The weight of the mandrel is much greater than the frame, therefore, the weight of the frame is considered insignificant in the model. The damping resistance represents the effective damping effect of the four rubber shock absorbers and the frame. The motors were neglected in the mechanical model since their weight was insignificant with respect to the mandrel and their eccentric mass was extremely small when compared to the motors' total weight. To find the vibration of the frame, a bond graph was developed and analyzed for the displacement of the frame as a function of the imposed forces. This is covered in detail in Appendix A.

Using the assumptions listed above, the following equation of a forced response to the implied load of the mandrel is obtained:

$$x = \frac{A}{\sqrt{(1 - \varepsilon^2)^2 + 4\eta^2\varepsilon^2}} \sin\left(\omega t - \tan^{-1}\left[\frac{2\eta\varepsilon}{1 - \varepsilon^2}\right]\right) \quad (2-1)$$

where

$$A = \frac{m_e \omega^2 r}{m} \text{ and} \quad \eta = \frac{\sqrt{km}}{2b} \quad (2-2)$$

This result shows that the displacement will lag behind the input force. To make the frame suitable for its function, the effective stiffness must be maximized and the eccentric mass minimized. By focusing on these two goals, any transmissibility resulting from operating the mandrel at or near the natural frequency will be greatly reduced. This approach was verified by modeling the frame on a finite element analysis program [Veeraraghavan, 1992]. The

deflections in the frame at different points could be summarized and the point of maximum deflection determined by representing the frame and its material properties on the computer and applying a static load. The static load was estimated at 25 kg and was evenly distributed on the two A-frames. The maximum deflections were nominally small and the frame was deemed stable.

3 THE MANDREL AND CARRIAGE ASSEMBLY

The mandrel is the rotating cylinder around which the filament wraps. It serves as a support for the developing composite cylinder and is affixed to the frame through bearings and a shaft driven via a belt system by a stepper motor. The mandrel has to meet several requirements to perform satisfactorily for the filament winding operations. It must be durable and solid enough to maintain structural stability when operating at a speed of approximately 720 rpm. The loads imposed on the mandrel are not only its own inertia, but also the force from the motor, pressure from the filament as it is wrapped around, and thermal stress while inside the radiation oven. The mandrel assembly is designed to support various electronic and mechanical equipment and, therefore, had to be designed to incorporate them. Construction of the cylinder considered the need to be a thermal insulator, neither giving nor receiving heat from the filament. Finally, the eccentric mass must be kept to a minimum on the mandrel. Since the mandrel is the largest rotating mass on the whole assembly, its eccentric mass would lead to vibrations and, subsequently, an unstable platform.

To ensure a well-machined filament winding machine with minimal eccentric loads, tolerances concerning the size of different machined parts were kept as small as possible during construction. Two major obstacles included designing for thermal expansion by the mandrel's construction materials and dealing with the limitations of the machining equipment.

The filament winding machine is designed to construct a composite cylinder of 17.8 cm inner diameter (ID) and lengths up to 36 cm. These dimensions were chosen since the Aerospace Engineering Department currently possesses equipment to conduct compression testing on cylinders of this inner diameter. Research into existing American Standards of Testing and Measuring (ASTM) codes did not provide any significant data confirming or contradicting the construction of 17.8 cm ID composite wound cylinders for standard testing so the decision was made based on existing facilities capabilities, enabling future students to establish a data base.

3.1 DETERMINING THE CONDUCTIVE HEAT LOSS

Steel was selected for the shaft and mandrel shell (Figures 3.1 and 3.2) for its durability, availability, and moderately low thermal expansion coefficient. However, steel has a low thermal conductivity and, therefore, is not an excellent insulator. A thermal insulator was needed to minimize the heat conduction of the mandrel assembly to the wound composite. The material of choice was a silicon refractory material called lava rock (Table 1.1). The lava rock was placed between the cylinder and shaft and serves as a barrier of heat transfer from the cylinder (see Figure B.2 in Appendix B).

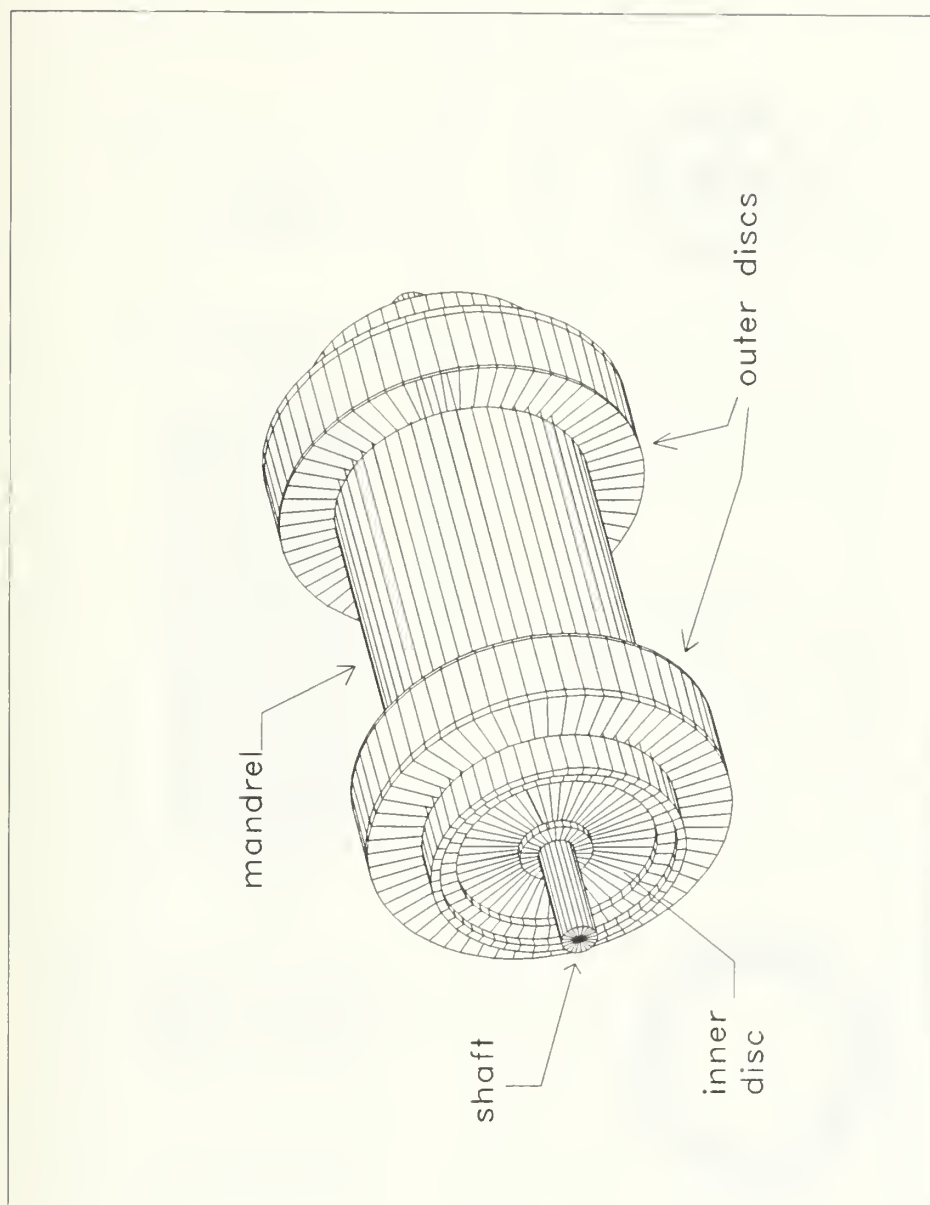


Figure 3.1: Mandrel (Three Dimensional View)

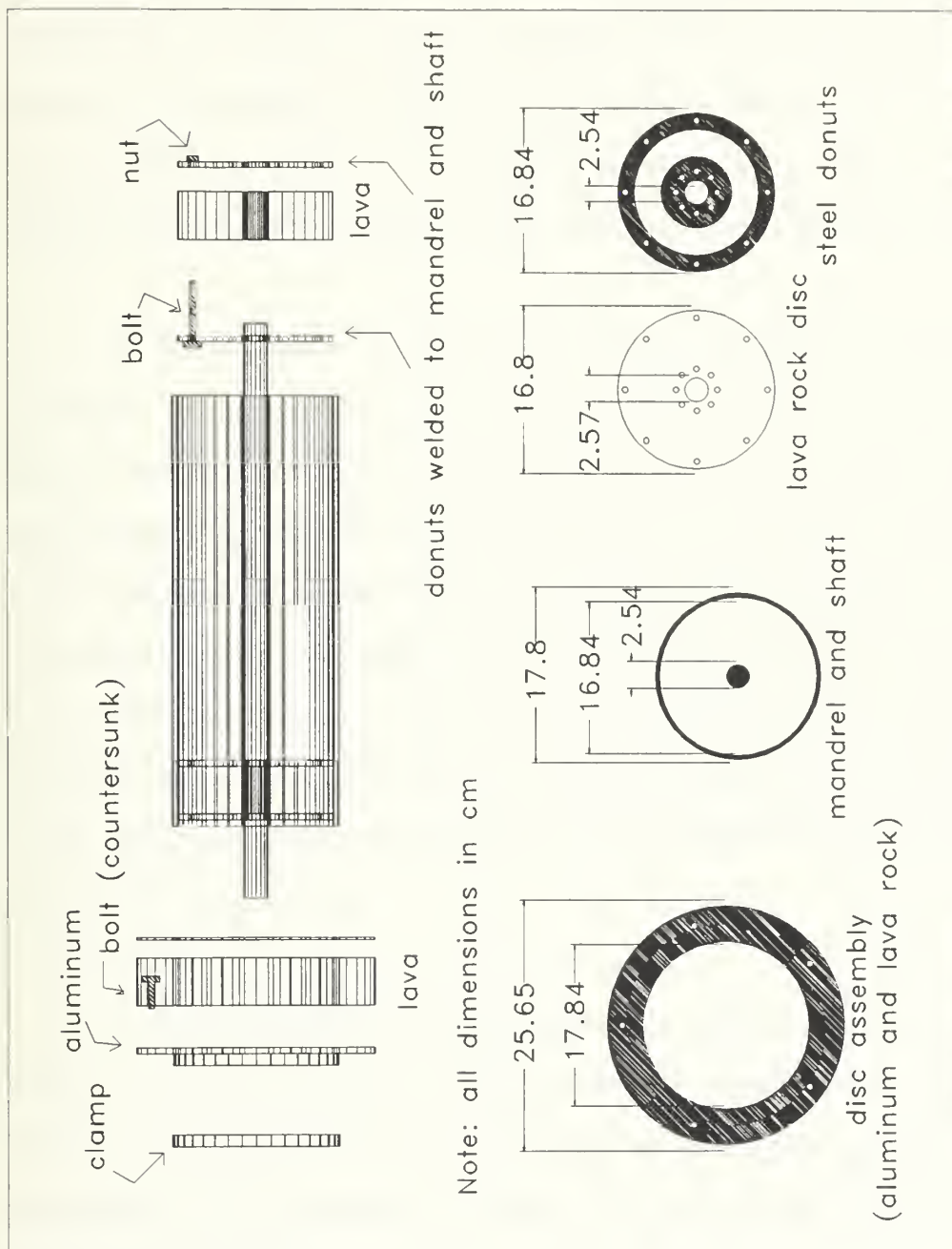


Figure 3.2: Mandrel (Scale)

Additionally, the refractory material supports the torsion force transmitted from the shaft to the cylinder inside the cylinder, where another thermal insulator is placed to further lower the thermal conductivity properties. This material is Kaowool Blanket Insulation. Its specifications are shown in Table 1.1. Blanket insulation was satisfactory since no additional structural strength was needed.

It was necessary to determine the thermal properties of the mandrel assembly. In order to do this, the radiative heat transfer of the oven to the filament was estimated. These analytical computations are covered in Appendix B and reflect the estimation of the thermal effect of the presence of the mandrel on the heat losses from the filament wound cylinder. By including the properties of the lava rock and blanket insulation and estimating the thermal conditions the mandrel and filament would endure to accomplish curing of the filament tape, the generalization was made that the conductive heat loss of the filament tape to the mandrel would be less than 5% of the radiation heat flux of the lamp bank to the filament tape.

Further discussions concerning the thermal properties of the project are in Chapter 5 which include the need to place heat shields on the lamp bank, develop an equation to compute the wasted heat, and develop a more accurate computation of the radiation view factor from the inferred lamp bank to the mandrel surface.

3.2 DIMENSIONING SPECIFIC MANDREL PARTS

After formulating the general design of the mandrel, the next step involved determining how the parts would fit together. The fixed dimensions on the mandrel included the shaft outside diameter (OD) of 2.54 cm, and the mandrel OD of 17.78 cm. Due to a fairly wide temperature operating range within the oven, a primary consideration was the difference in thermal expansion between the steel and refractory material. The steel and refractory could not be press fit together or the lava rock would crack. The next option was to predict the expansion and contraction of the different parts expand and make an allowance in the design. Specific analysis is included in Appendix C.

3.3 CALCULATING POTENTIAL SLIP OF THE FILAMENT WRAP

Another important issue concerned affixing the filament tape or wrap to the mandrel. The design intention was to allow cylinders to be formed by helical or hoop winding, or any variation in between. The type of winding is determined by the rotation of the mandrel relative to the carriage assembly. A review of the dynamics of the filament tape as it winds onto the mandrel found that a tow tension is imposed on the material (Figure 3.3). This tow tension is necessary to insure no slop incurs during the winding operation. This force is provided by a tensioning system. However, the axial component of the tension may cause slippage along the length of the mandrel.

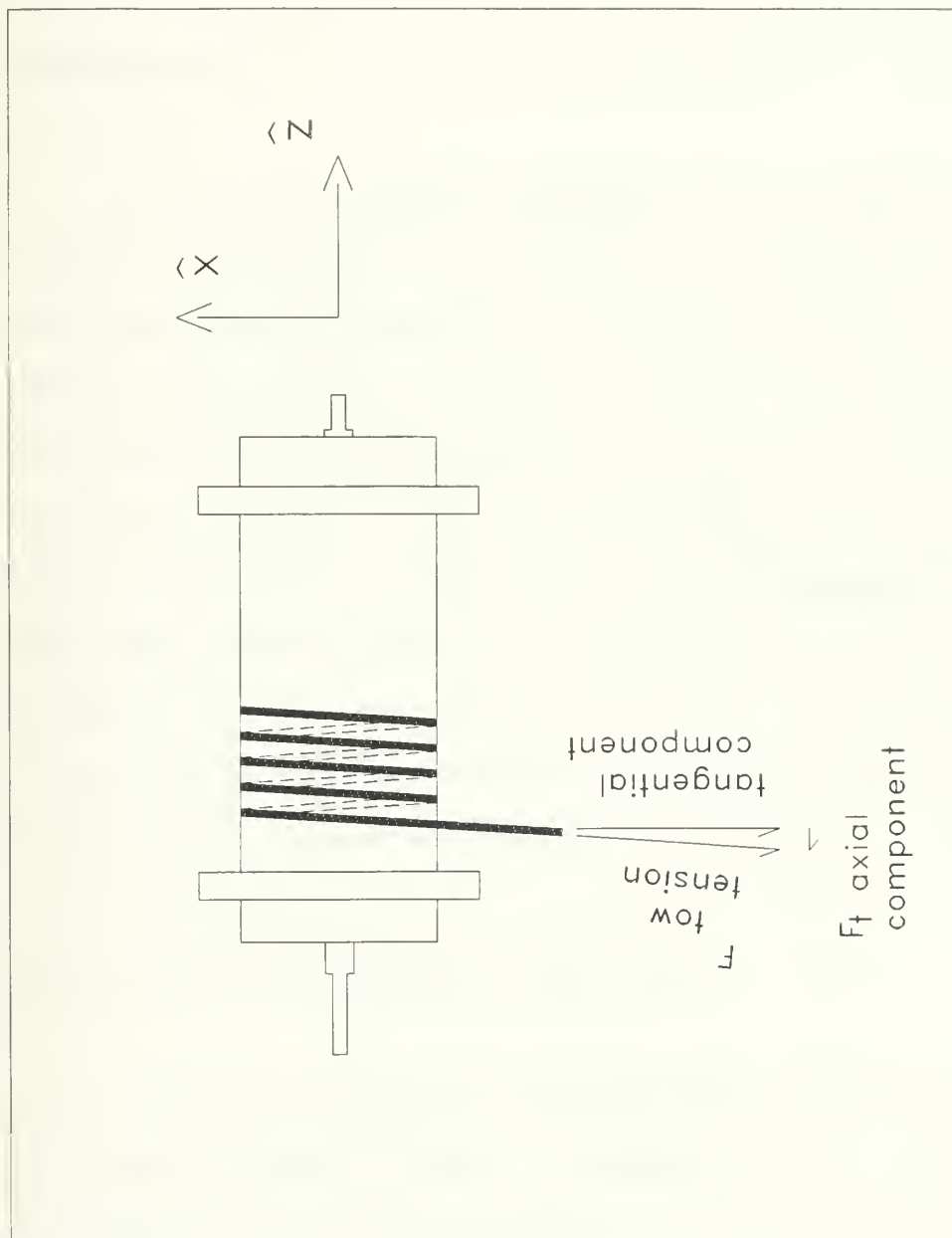


Figure 3.3: Filament Tow Around Mandrel

The strength of the finished product is highly dependent on minimizing air pockets and wavy tows, and can only be accomplished if the placement of each tow is precise. Slippage interferes with this placement effort and weakens the finished product.

The only way to minimize the slippage is to have a higher fictional force keep the filament in place as it wraps onto the mandrel. This becomes a critical factor when the filament winds all the way to the edge and starts back in the other direction (see Figure D.1 in Appendix D). To look at this problem analytically, specific conditions were identified that may exist in a winding operation. A prepreg tape with a 0.46 cm width was on hand and used to conduct a helical winding experiment. Study of the dimensions of the filament, the winding angle (θ), and the necessary tension required to be applied to the filament as it is wound showed that serious slippage would not be a problem. This argument is in Appendix D and is only valid for the conditions specified. A recomputation is necessary with any change in the variables.

3.4 STRENGTH COMPUTATION OF THE DISC LIP

The filament is bounded by two discs affixed to the mandrel via a clamp. The discs are made of aluminum and refractory material to provide a rigid boundary as the filament thickness increases during the winding operation and to minimize any heat transfer to or from the filament. As with the construction of the mandrel, the aluminum is horizontally bolted to the refractory material in a

manner to allow for the difference in thermal expansion as the two are heated. The discs contain lips over which the clamps slide and lock. Set screws in the clamps make contact with the lips and press them onto the mandrel. This combination insures a secure fit of the disc to the mandrel with little chance of slippage.

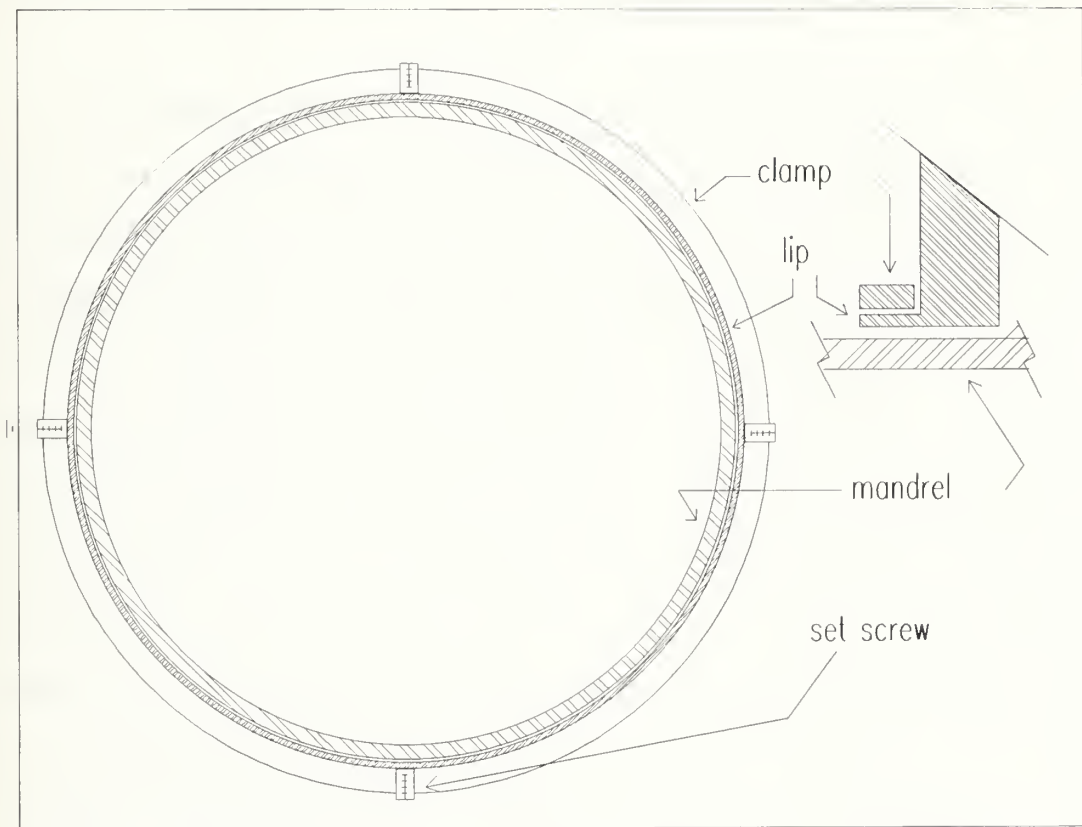


Figure 3.4: Clamp (Top View and Section)

The tolerances during the machining process dictate a lip deformation of approximately 0.05 inches before contact with the cylinder. The lip is very thin, therefore, its fragility is of importance to insure that it will not snap off at the

base. The analysis of the lip is covered in Appendix E. From the results of the computations, it can be concluded that the lip would suffer permanent deformation but would not fail. Consequently, the dimensions of the lip are satisfactory for affixing a clamp and restraining the outer discs to the mandrel.

3.5 THE CARRIAGE ASSEMBLY

A carriage assembly was needed for the filament winding machine to establish the winding pattern of the filament and to direct with precise accuracy where the filament should lay on the rotating mandrel. The carriage assembly consists of two parts; (1) a single degree of freedom rail table and (2) a roller assembly. The rail table is connected directly to the stepper motor. The stepper motor moves the platform on the rail table via a screw. The roller assembly is connected directly to the platform. Figure 3.5 shows the layout of the roller assembly, which is constructed with two sets of rollers. One set directs filament of any width up to 0.75 inches (1.9 cm); the second set directs filament with a width up to 3 inches (7.6 cm). The second set was constructed to accommodate experiments dealing with filament winding with no carriage movement. The first set of rollers is designed to direct filament placement with transverse patterns. Consequently, the rollers are concave. This design keeps the filament in the center of the roller and minimizes unwanted lateral movement of the filament with respect to the carriage assembly as it transverses the rail table.

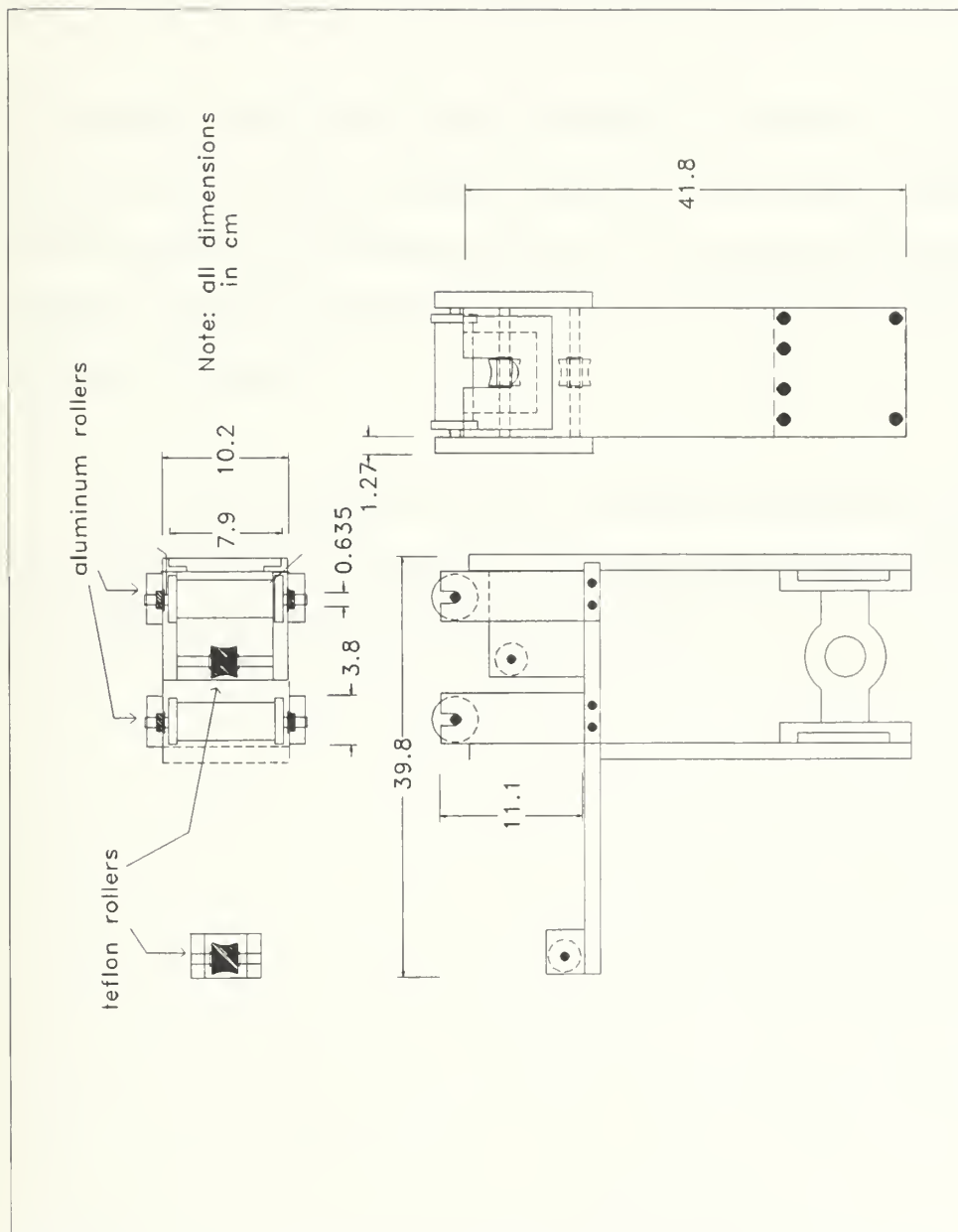


Figure 3.5: Carriage Assembly (Scale)

This design works only when there is a specified tension on the filament tape from a tensioning system which is separate from the carriage assembly.

The predicted tensioning load is not to exceed 5 lbf (22.25 N). The motor to drive the carriage must be accurate enough to allow precise positioning and lateral displacement, yet strong enough to move the carriage with instantaneous acceleration and various velocities. The sizing and procurement of the motor is discussed in Chapter 7.

The carriage assembly is made of aluminum and fastened with bolts. Since no great stresses are placed on the assembly, the design will suffice as a stand-alone fixture and require no additional support.

4 THE THERMOCOUPLE ASSEMBLY

An operational requirement of the filament winding machine is to measure the temperature of the filament during the winding operation. Ideally, the temperature at numerous locations could be determined, but this goal greatly increases the complexity and expense of the experimental equipment. With this in mind, the decision was made that monitoring the temperature of the filament at only two locations would provide satisfactory feedback on the dynamic temperature profiles. Since the thickness of the finished product will be approximately 0.50 inch (1.27 cm), a method was devised to insert a small thermocouple in the developing cylinder when it reached a specified thickness of 0.25 inch (0.635 cm), thereby monitoring the temperature of the filament tape at that specified location for the next 40-60 revolutions of the mandrel. The size of the thermocouple is important. A thermocouple that is too small might transmit an inaccurate reading; if too big, it would create an air pocket between the layers of filament tape, creating a temperature signal inconsistent with actual temperature of the filament tape at that specified location. The solution to this problem was to use a thermocouple with a diameter smaller than the filament thickness, which still maintained design characteristics within the expected temperature parameters.

Once a proper size thermocouple was found, the next step involved determining how to inject the thermocouple into the filament and then read and record the temperature. Because the filament revolves with the mandrel, simple

wires leading from the thermocouple to the stationary data acquisition system (DAS) were out of the question. The design solution was developed by Chin Seng Chu and is shown in Figure 4.1.

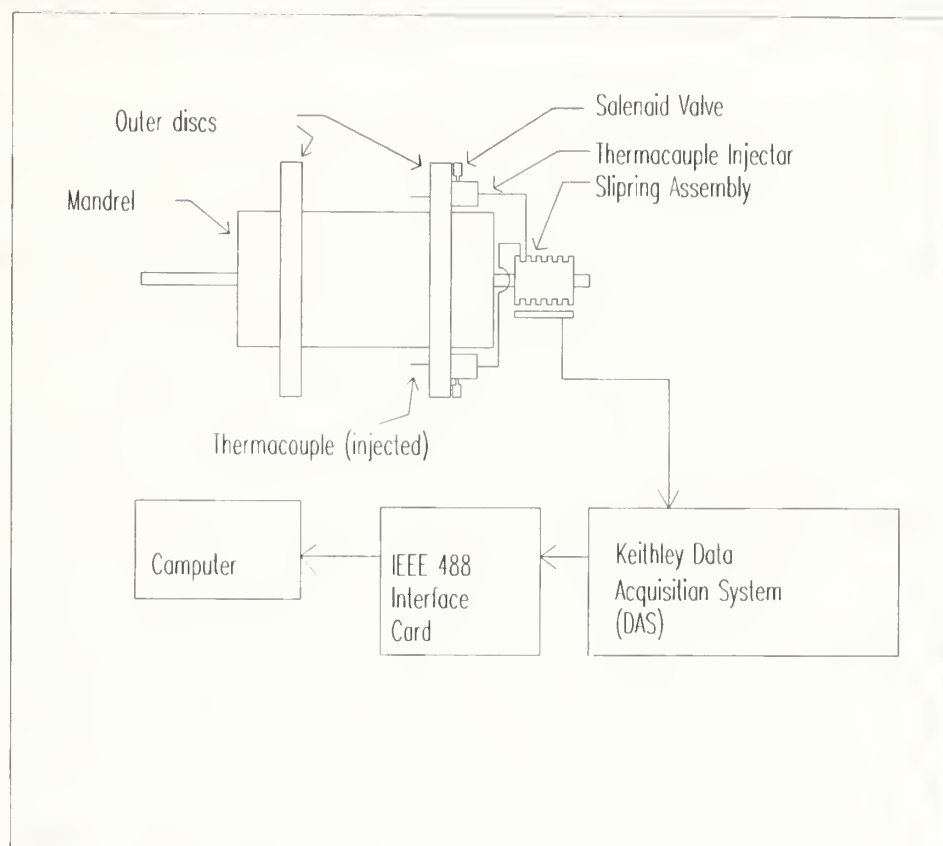


Figure 4.1: Thermocouple Acquisition System

The thermocouple is affixed to a piston, which is spring loaded and actuated by a solenoid. The piston is held back by the pull-type solenoid. During the winding evolution, a signal is sent to the solenoid at a predetermined time. The solenoid activates, releasing the piston which shoots forward sending the exposed thermocouple into the winding region of the mandrel. The

thermocouple stays exposed until subsequent layers of filament tape cover it from above and compress it into the layers below. The thermocouple remains sandwiched between these layers and reads the local temperature. The thermocouple signal is fed through a slipping assembly and finally to the DAS.

Success of this apparatus depends on knowledge of thermocouple assemblies and the restrictions imposed by them. Thermocouple wires are composed of different metals and must be connected to each other to generate a signal. When soldered, a third metal is introduced into the thermocouple assembly. To insure this third metal does not introduce an error into any readings, the two primary metals (wires) must be at the same temperature when conducting readings. This is usually not a problem but appropriate experimental conditions must be maintained. Moreover, solder remains solid only over a specific temperature range. Welding of the two primary wires is preferable if high temperature readings are required. The welding operation must be conducted with care since overheating the wires can change the thermal characteristics. A K-type thermocouple is employed in these experiments.

Thermocouple wires must be in good condition and well protected with insulation at all points except the ends, which measure the temperature. Mishandling and improper storage can expose the wires, causing a diffusion of atmospheric particles into the metal and subsequently lead to decalibration. Improper installation and insufficient insulation (such as wrapping the bare thermocouple wires around a heated copper tube) can induce unwanted

temperature gradients on the wires. Since the thermocouple wires produce a voltage as a function of the temperature being read at the junction, an induced temperature gradient along the path of either or both of the wires can alter that voltage and again lead to an inaccurate reading. Therefore, insulated wire is used in this experiment to protect against contact with metal surfaces while the wire travels back to the signal processing equipment.

The diameter of the wires used is very small and leads to dependence on another aspect of adequate insulation. Insulation protects the thermocouple wires from both outside influence and each other. For example, if a pair of wires is encapsulated in a protected coating, the electrical voltage which may travel between the two is impeded by the resistance (\bar{R}_L) of the combined coating on both wires. If the wire is small enough, its resistance ($\bar{R}_{s1}, \bar{R}_{s2}$) may be quite high. The resistance of the coatings can decrease exponentially as temperatures increase. This may lead to a condition such that $\bar{R}_L \ll \bar{R}_s$ and subsequently cause one wire to transmit its voltage to the other wire (see Figure 4.2) [Omega, 1989]. The wires and insulation were chosen to ensure the coating resistance between the wires is sufficiently high so the two wires remain electrically insulated throughout the experiments.

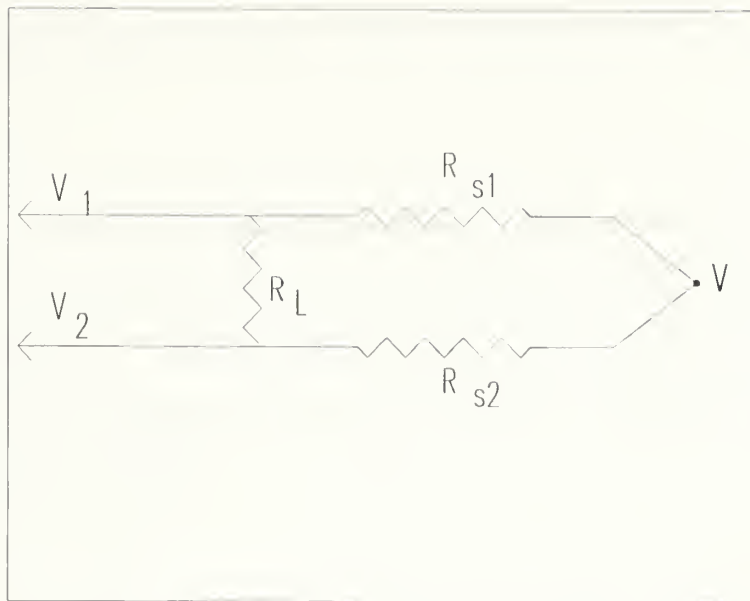


Figure 4.2: Resistance in a Thermocouple Wire

In addition to electrical shunting, thermal shunting was also a concern in the experimentation. The filament wrap to be measured was only 0.14 cm thick. A thermocouple with a large mass relative to the object being measured alters the temperature of that object. In this specific experiment, a large thermocouple would also produce significant air pockets in between the layers of wrap where the thermocouple is sandwiched. It was therefore necessary to use a thermocouple with a small mass relative to the wrap. As previously discussed, the problem of shunt impedance may become an issue if the wrap is too small. This problem was prevented by choosing the largest wire possible which would still be smaller than the thickness of a single filament wrap. This action helped minimize the size of the air pocket created on either side of the thermocouple as it is sandwiched between the layers of wrap. Subsequent

examination led to the conclusion that a wire size of 0.08 cm was the best choice.

After selecting the appropriate thermocouple system, a method was needed to inject the thermocouples into the filament wound cylinder during the winding operation. Successful insertion would enable monitoring the temperature of the filament tape and recording its variations as the mandrel spins under the lamp bank.

Figure 4.3 is a plan view of the injection assembly designed for this job. The design consists of spring loaded pistons inside cylinders. The cylinders are permanently attached to the large outer discs of the mandrel. The pistons are pushed against the far wall of the cylinder and the spring is compressed. The piston is held in place by a pull type solenoid. The solenoid is connected to an encoder and a counter via a slipring assembly. The thermocouples are also connected to a DAS via the same slipring assembly. When the filament winding machine is running and the mandrel is spinning, the counter records how many revolutions the mandrel makes and, consequently, the number of times the filament tape has been wrapped around the mandrel. At a predetermined revolution count, the counter sends a signal to each solenoid instructing it to retract, thereby releasing the pistons and propelling the thermocouples into the area of the mandrel where the filament tape is being wrapped. The thickness of the filament tape already wrapped on the mandrel is such that the thermocouples have a clear path and are not pushed into the filament tape.

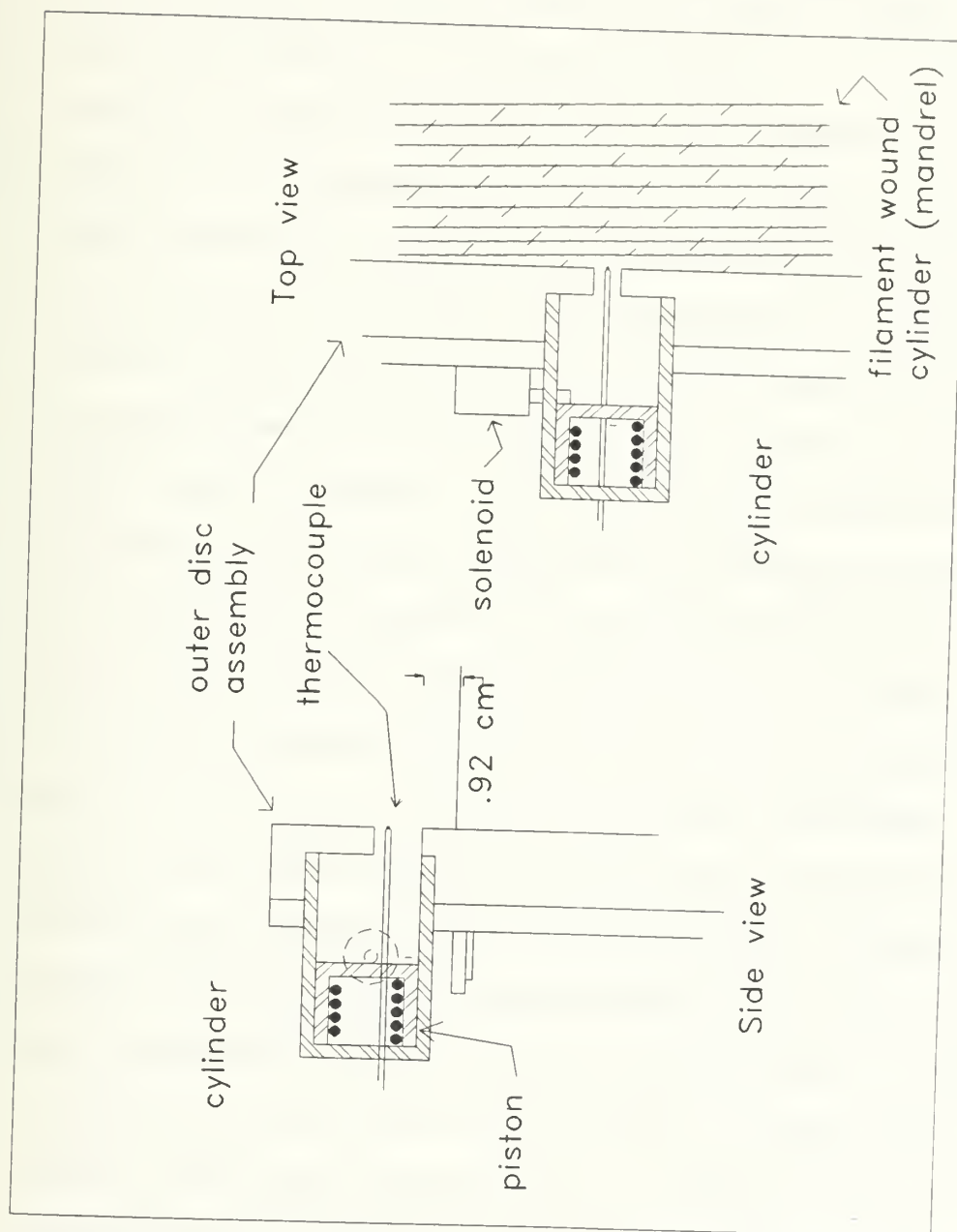


Figure 4.3: Thermocouple Injection Assembly

Once the thermocouples have traveled their full extension of 1.75 inches (4.45 cm), the next layers of filament tape lay over them and secure them to the cylinder being formed. From the time of insertion to the conclusion of the winding, the thermocouples measure the local temperature of the wound cylinder and send a signal back to the DAS. The slipping assembly must be highly accurate and not subject to a significant amount of noise to perform this task accurately. The electrical signal that triggers the solenoids must be momentary and then terminate since it is a large voltage reading compared to the millivolt signals sent by the thermocouples. Interference of one signal onto another must be prevented. The thermocouples are disposable and are cut loose from the filament wound cylinder after the experiment and replaced with new ones for the next experiment. The solenoids must be secure enough to hold the piston in place while the mandrel is turning, yet strong enough to retract fully when called to do so. Only two can be safely attached to the outer disc due to the size and weight of these injection assemblies. They are attached to the disc at diametrically opposite ends to minimize the chance of vibrations due to eccentric mass. The slipping assembly must have at least 8 electrical contacts since each injection assembly needs four (two for each thermocouple and two for each injector) to operate properly. Construction of the assemblies must be precise and the cylinder and piston walls smooth to minimize friction and unnecessary force. Additionally, the travel of the thermocouples must be large enough so that temperature readings can be taken in the "interior" of the two and negate end effects of the filament touching the disc walls. Since the future experiments will involve hoop-winding filament

tape of 3 inches in width, a thermocouple injected 1.5 inches provided the most accurate readings.

Since a wire with an extremely small diameter was used, it was necessary to insure that the centrifugal forces of the mandrel would not have any adverse effects of the wire. Specifically, the wire should not bend significantly and preclude its insertion into the filament wrap during the winding.

Analysis of the deflection of the thermocouple is covered in Appendix F. Solving for the maximum deflection showed that the deflection of the thermocouple due to the spinning of the mandrel would be insignificant.

5 THE HEAT SHIELD

As discussed in Chapter 3, the filament tape on the mandrel is heated continuously by IR lamps during the winding operation. One issue not yet reviewed is what happens to the rest of the filament winder when exposed to the elevated temperatures of the IR oven. As will be shown later, the filament winder contains temperature sensitive equipment which must be protected as much as possible. After considering numerous alternatives, the author concluded that the best protection will be provided with the addition of heat shields to the lamp bank as shown in Figure 5.1.

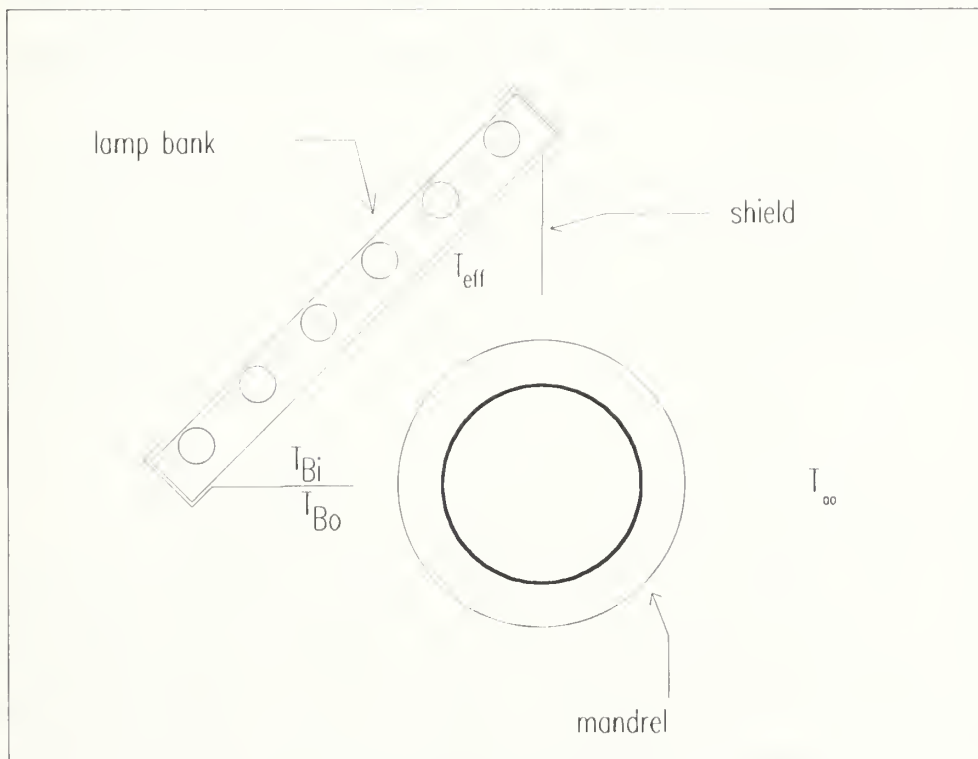


Figure 5.1: Mandrel Positioned under the Lamp Bank

By installing these shields and coating the heat exposed side with a low emissivity foil, the design should reflect much of the radiation heat and minimize transmission through the shield to the operational components of the winder. Using the design, the heat flux was estimated from the lamp bank to the surrounding area and the temperature predicted of the heat shields during steady state operation. This analysis is covered in Appendix G and demonstrates that sufficient heat flux can be directed onto the mandrel as long as the following conditions apply:

- 1) The lamp bank is properly sized for the mandrel.
- 2) A highly reflective surface is used to coat the inside of the shields.
- 3) Forced convection is used to dissipate the heat from the shields.

Unfortunately, the efficiency of the system is reduced when the lamp bank is much larger than the area to be radiated. This occurs with installation of additional shields to block or divert heat away from the mandrel and its supporting equipment.

As an additional measure, the view factor between the active heat source and the exposed portion of the mandrel is computed. The previous problem which dealt with the heat flux was two dimensional because it gave a representative analysis on what to expect in the way of shield temperature and heat flow. However, a more accurate model must be developed to determine

the view factor in order to derive useful information. The view factor problem is three dimensional and is discussed in Appendix H.

The view factor is concluded to be extremely small based on the analysis. The analysis indicates only 5% of the heat flux emitted from the source will directly reach the mandrel. Recalculation of the equation with a smaller distance between the heat source and the mandrel did not markedly improve the view factor. An increase in source area increases the view factor but also decreases the heat flux, thereby having no significant overall effect. Hence, the direct efficiency of this setup is very low and the need arises to rely on a significant amount of light reflecting downward from the shield sides to increase the overall heat transfer, a factor that is extremely difficult to compute analytically and can only be measured experimentally.

6 MACHINING

During the design of a mechanism or a part, the designer must be conscience of the method and effort level necessary for machining a given part. A design and its corresponding analytical calculations are worthless if they cannot be applied to anything more than the paper they are written on. Additionally, even though the versatility of a machine shop and the experience of the machinists may allow the custom production of almost any part, time and effort are a serious consideration. Tool machining is a highly technical, specialized profession and is subsequently an expensive operation both in terms of equipment and man-hours expended. Parts must be designed for economical production and have tolerances that are realistically obtainable. If not, no degree of innovative thinking behind the desk can make the part worth producing and the design becomes nothing more than an exercise in expending time fruitlessly. Additionally, without considering applied engineering practices and precise instrumentation of the machining equipment, no theoretical research can be tested and analyzed in the field and the research is only valid as far as the rudimentary equations it is based upon.

Due to externally-imposed time constraints for the design and construction of the filament winding machine, the author started with a conceptual design and refined it during construction. It was during the construction that all the analytical calculations were applied. A combination of traditional practices and ingenuity were used to fabricate the parts.

Although machining is an in-depth and highly skilled profession, the applications necessary for the project were fairly basic. Three primary pieces of equipment were employed: a lathe, a mill, and a bandsaw in the Mechanical Engineering Department Machine Shop. The bandsaw was employed for rough cutting material to approximate size. The mill took these pieces and machined them to a fine tolerance suitable for the application. The lathe was used for turning stock to produce cylinders, shafts, and all rotating pieces of equipment.

With each piece of equipment, the majority of the shop time was spent on setup. The setup of the equipment is especially important since the required tolerances of the finished product could not exceed $\pm 3\text{mm}$ in most cases and sometimes less. Before any machine was used, it was checked for accuracy and squareness. Proper care was taken in securing the work to the equipment using standard procedures for the type of cutting at hand. Often the material was secured using common attachments such as the lathe chuck and the center on the engine lathe, but sometimes special fixtures were machined to secure the work in positions uncommon for machining. For example, a steady rest was needed when turning the mandrel shell. The steel cylinder (in its original form) was large and could not be held secure using a lathe chuck alone. The steady rest served to secure the cylinder from the outside on the end of the cylinder away from the chuck. Since the steady rest held the cylinder at three points and an error of accuracy could occur in two degrees of freedom, much time and effort were invested to align the outside of the cylinder length such that it would be perfectly parallel to the path of the cutting tool. This led to another

important lesson in machining. When a piece of material is set up and positioned for cutting, it is highly recommended that all work is finished on that piece before it is removed from the machine. By removing and reinstalling a piece in a lathe or mill, additional time is invested to reset the equipment and it is difficult to exactly match the position of the piece relative to the previous setup. Any cuts made after the reinstallation will always maintain a margin or error relative to the initial setup and cutting.

Sometimes custom clamps or holding fixtures were machined and fitted into the primary object to be worked. One example is cutting the discs to fit inside the mandrel. The original steel plates could not be held by a chuck so driver plates were manufactured with dimensions suitable for holding them securely, while allowing enough clearance between the plate and chuck to allow passes with the cutting tool. Again, the accuracy of these custom fixtures were paramount since they affected the accuracy of the finished product.

When machining, special care was taken to insure proper settings on the equipment. The cutting feed rate is dependent on the material being used. In addition, tools and bits are designed for different types of material. The primary working material was low and medium carbon steel, a variety of aluminum alloys, and Teflon. The cutting speeds for the steel were approximately 24-36 meters per minute (mpm) while the speeds for the aluminum increased to 60-90 mpm. These ratings are identified as the linear velocity of the cutting tool over

the material. When drilling or turning a piece of material, these linear velocities must be converted into rotational speeds and applied accordingly.

Drilling was a prevalent exercise in the construction of the filament winding machine and specific rules concerning setup and operation were followed to insure accurate and precise operations. Drilling is a process by which a hole is originated or enlarged by a specific type of revolving end-cutting tool. Most drilling was conducted on an end mill which allowed very precise positioning and all drills were two fluted standard stock. The material to be drilled is rigidly clamped before proceeding. All holes are initiated with a center drill which provides a focused indentation for the drill bit and minimizes any chance of the drill wandering or bending when it comes into contact with the material. When drilling, the chips are removed via the recesses between the flutes. It is imperative that while drilling, the bit is frequently retracted from the work and the accumulated chips are cleaned away. If this is not done, clogging of the bit could occur which would lead to breakage of the drill bit.

Most of the machine was fastened together with welds or bolts. Subsequently, a general understanding of bolts and screws was necessary to insure proper techniques were followed when connecting members. It is impractical to conduct specific stress measurements on every bolt so it was necessary to standardize the bolts used and analyze the members being connected to ensure the bolts met or exceeded the tolerances to be placed upon them. With few exceptions, all bolts maintain American Standards and are

manufactured under the American Standard Unified-Thread Form. Figure 6.1 highlights some of the characteristics of each bolt.

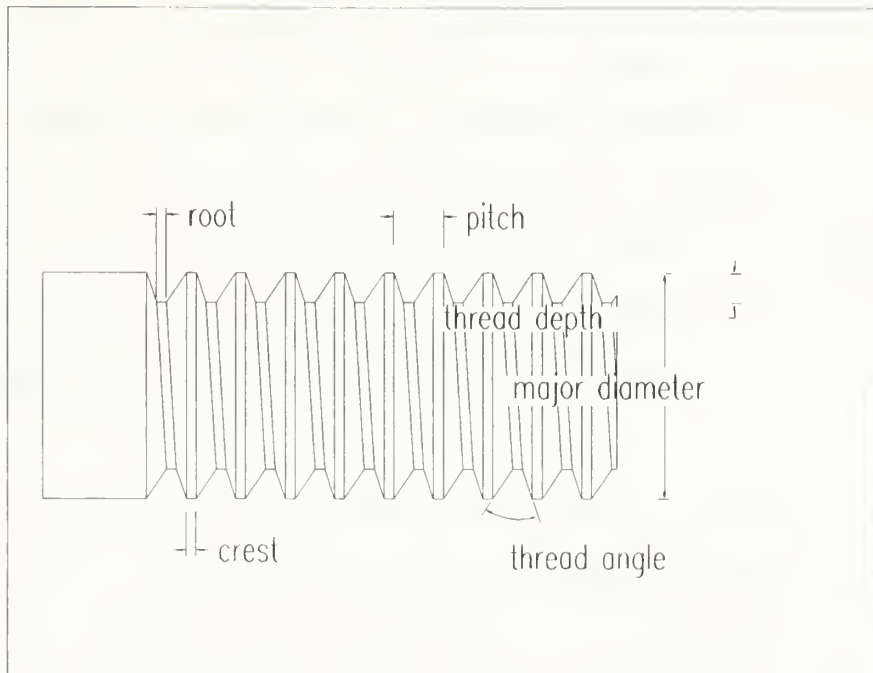


Figure 6.1: Bolt Characteristics

The primary dimensions are the relationships between the major diameter and the threads per inch. For example, most of the bolts used had an outside diameter 0.25 inch (0.635 cm) with 20 threads per inch. By reviewing the Machinery Handbook on these bolts and using low carbon steel with a coarse-threaded series, the tensile stress area was calculated at approximately 0.25 cm^2 and the minimum tensile strength of the material was 3.8 EE8 Pa , giving an adequate 7800 N of force for each bolt [Ryffel, Green, Geronimo, 1989]. Also of considerable importance was the fact that bolts are always placed under preloading when they are attached to a member and that a specific amount of

torque is applied. In a rigid joint, the tension must be greater than any external loads applied. If the bolt is tightened to produce 4000 N of tension in the bolt, a load up to 4000 N. can be applied to this assembly without causing additional loading in the bolt. As the bolt is preloaded, it elongates. This preload is applied via torquing the bolt and must be maintained throughout the life of the joint. Factors which can undermine this preload are accumulation of rust, surface burrs, inadequate matching of parts or foreign matter. As the bolt loses its elongation, it will lose its prestress. It will stay tight as long as external loads are within the preload limit, then lose its effectiveness.

In non rigid joints, such as gasket joints or ones containing a damping medium, the bolts must have enough strength to take the preload plus any additional load. The bolts in these joints must be tight enough to resist the operating forces and to maintain a tight fit when the machine is at rest. Again, as long as the maximum forces do not exceed the design stresses of the bolt, repeated loading will not cause fatigue or loosen the joint.

Preloading also provides a locking effect to avoid unscrewing. Excessive amplitude of stress change in a bolt may cause the nut to loosen. Proper tightening is the recommended way to keep a nut on a bolt. If the preload is sufficient, the fictional forces exerted on the contracting surfaces will resist shear and there is no slippage. For the bolts in this project, a minimum torque limit of 55-66 in-lb (6.2-7.4 J) was within specifications and was satisfactory for these applications.

It is was very important to check the depth of the hole on the bolt connections to ensure it was at least twice the width of the bolt diameter (see Figure 6.2). For example, bolts with a 0.635 cm diameter were never applied to join pieces with a combined hole depth of less than 1.27 cm. This was necessary to guarantee enough metal in the rigid joint to accept the forces the bolt imposed on it. In the case of tapping the hole with threads, the depth of the hole determined how many threads would be cut to hold the bolt in place.

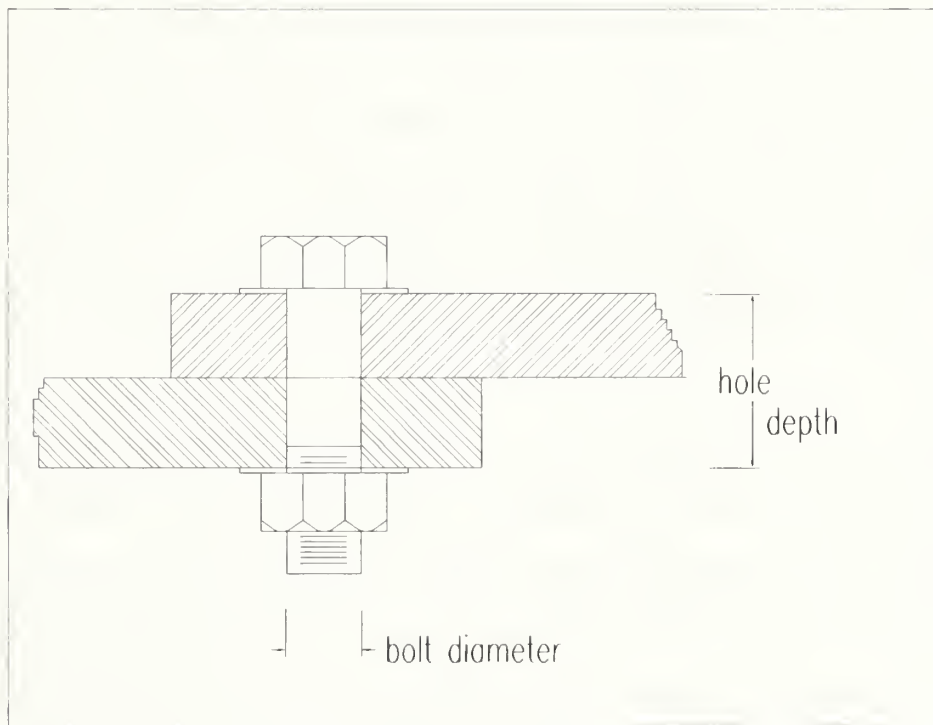


Figure 6.2: Bolt Diameter vs Depth of Hole

If the threads were insufficient, the steel member could not restrain the bolt once a load was applied and the threads would shear off [Machinability Data Center, 1979].

Tapping a hole is the practice of creating a hole and threads in the metal to receive the bolt. Again, standard bolts have standard threads and the initial hole must have a specified diameter such that the tapping tool can effectively create the threads with the proper inside and outside diameter and proper pitch. By the standards set forth in manufacturing bolts, a bolt is designed so that a satisfactory grip is maintained if 50% of its thread is in contact with the threads of the hole. In other words, if this bolt in question is loaded beyond its design capacity, the bolt will break before its threads are stripped off. In practice, holes are tapped to insure contact between the bolt and hole extends to 75% of the bolt's thread length. A full-depth thread is only about 5% stronger than a 75% depth thread, yet it requires three times the power to tap. In this project, the 75% thread depth rule was followed for safety and economical tapping.

Press fitting of two cylinders was a common practice when a secure bond was needed. When press fitting, a specified interference between the inside diameter of the larger cylinder and the outside diameter of the smaller cylinder was required to insure sufficient frictional forces to prevent slippage. This interference had to be precise and the surfaces of the cylinders had to be exceptionally smooth. If the first of these conditions was not met, the force needed to press the two objects would be excessive. If the second was not met, the bond between the two would not be secure and the two cylinders would be unparallel. The cutting of the outside diameter was performed on the lathe. To obtain the exact tolerances, small cuts were taken and a slow

automatic travel speed was applied relative to the rotational speed of the piece being cut. This, in effect, polished the outside diameter. Once the part was cut, the inside diameter of the adjoining cylinder was created by first drilling a hole and then reaming the hole to the diameter needed. The reamer gives the operator the ability to cut the hole to an exacting dimension and provides the necessary smooth surface. As a result, reamers are fragile tools which can easily be damaged. For example, failure to rotate a reamer in the forward or cutting direction will damage the margin and alter its accuracy. The desired interference between the outer and inner diameter of two cylinders to be press fit is 3 mm. Since reamers come in standard sizes, the interference dimensions must be based off of the reamer size to be used.

7 THE MOTION CONTROL SYSTEM

Designing and procuring a motion control system for the filament winding machine was the most expensive single item in this project. Therefore, care was taken to identify and procure the right system or face a costly mistake. The specifications and design parameters for the motion control system were identified early to allow sufficient time to shop around and identify the best product for the requirement. From the design parameters of the winding machine discussed thus far, a review can be made of the specifications to gain an understanding of the operational requirements.

In general, the motion control system must provide a two axis coordinated movement on the filament winding machine: one for the mandrel rotation and the other for the repeated lateral movement of the carriage assembly. In order to produce specific winding patterns, the motors must be coordinated by one controller having simultaneous control over both motors.

The motors for the system had to be durable, accurate with respect to position, and powerful enough to handle the torques and accelerations needed. Durability was a requirement since the working environment is hostile to the extent that ambient temperatures may be high and the working area unsanitized. Accuracy was needed so that the position of the motors, and consequently the mandrel and carriage, could be determined and monitored on a constant basis. Adequate power was a crucial requirement since the 25 kg mandrel had to

reach a speed of 720 rpm with accelerations greater than 15 rev/sec^2 . The option included using stepper or servo motors. A servo motor consists of a magnetized rotor encompassed by windings on the stator poles. AC current is continuously reversed throughout and an electronic amplifier which operates in response to a low-level signal from an optical sensor or encoder. To rotate the motor, the current in the external circuit must be reversed at defined rotor positions. A stepper motor, on the other hand, receives input signals as step pulses and a direction signal. One step pulse is required for every step the motor is to take. For most industrial use stepper motors, the stepping mode is the half-step mode in which the motor performs 400 steps per revolution, but this could be increased to 50,000 steps per revolution depending on the accuracy required. Stepping motors are generally more powerful with respect to their size than servo motors but servo motors dominate in the field of accuracy [Compumotor, 1991]. To minimize the complexity of the system, stepper motors were used to eliminate the need for encoders. Although encoders would give feedback to the operating system in terms of position and velocity, a stepper motor properly designed for the application would be as accurate in the sense that it would take the positioning and acceleration commands from the driver and meet those inputs without any need for feedback. Concerning position, motors will be acquired with the positioning capability of 25,000 steps per revolution (0.0144 degrees per step). Of course, as the accuracy increases, the torque available decreases.

Power requirements for the system was an issue to consider. It was found from earlier experiments that the laboratory may be unable to accommodate equipment with an unusual power demand (i.e. 220 V, single phase). Connections and modifications of existing electrical systems were costly, time consuming, and inefficient. This made it important to check the power requirements to ensure accommodation of any new equipment. In the case of the motion control system, it was necessary that the system run on 115V AC, thus ensuring that power would be available.

Since the operating environment of the filament winding machine is an IR oven, the motors have to withstand high temperatures. The conditions to which the motion control system can be exposed were set realistically. After review of the different products and their capabilities, a limit of 50° C (323 K) was set for the maximum temperature under which a motor was expected to operate.

The motion control system had to be a self contained unit. In other words, the hardware and software had to be complete and integrated. Therefore, the supplying manufacturer would be available to answer any questions or necessary troubleshooting.

In determining the size of the motors, the torque requirements were computed and motors found to match the torque and velocity requirements with a sufficient safety factor; hence, the motors had to exceed the minimum requirements by a specified amount. This allows flexibility concerning future

applications, anticipate unforeseen and unpredicted loads, and insure longevity of the system. This analysis is covered in Appendix I.

Another specification placed on the future motion control system is the need to have user friendly software for programming. The future operators of this system may not possess an in-depth knowledge of different programming languages. Therefore, a straight forward applications program will be beneficial in developing and running winding operations.

Table 7.1 details some of the specifications of the motion control system procured for the filament winding machine. All motor requirements were met and the system was compatible for this use. The controller, or indexer, runs the program and sends signals to the drivers which in turn send electrical signals to the motors setting the acceleration, velocity, and direction parameters. The motors are stepper motors and therefore do not employ encoders. The design operating temperature is 50° C.

TABLE 7.1
MOTION CONTROL SYSTEM SPECIFICATIONS

1. Indexer (Controller)

degrees of freedom	1 or 2
support software	MS-DOS
memory	40,000 bytes
power input	120 - 240 VAC
input/output capability	24 programmable

2. Motors and Drivers

	a) S83-135	b) S57-51
static torque	400 (3.21)	65 oz-in (.46 N m)
rotor inertia	10.24 (1.87)	.48 oz-in ² (.088 kg cm ²)
bearings (thrust)	50 (22.6)	25 lb (11.3 kg)
bearings (radial)	25 (11.3)	15 lb (6.8 kg)
radial play	8E-4 (.002)	8 EE -4 in (.002 cm)
weight	8.3 (3.8)	1.6 lb (.7 kg)

8 EXPERIMENTATION AND RESULTS

With the machining and construction complete, the filament winding machine was relocated to Balcones Research Center and placed inside an IR oven (Appendix J). Four software programs were written for the motion control system. These programs instructed the filament winding machine to perform specific motions and were developed in support of winding operations of to test the capabilities of the machine itself.

The mandrel was tested for high velocity operations and rotational speeds of 640 rpm were obtained. Unfortunately, the tests showed that the main shaft of the mandrel was slightly bent. This deformation (which is surmised to have occurred during construction) caused parts of the shaft to be off centered. The deviations were most serious where an encoder and slipring assembly were affixed to the shaft. The off centered deviations for the encoder and slipring were 0.015 cm and 0.03cm respectively. Although noticeable, this situation is correctable but the process is time consuming. The shaft can be straightened by detaching it from the filament winding machine and placing it under an end mill. The mandrel can be firmly secured and the bends in the shaft taken out by applying force on the shaft. In the current experiments, however, this is not necessary. The bent shaft gave no indication of adversely affecting the functions of the slipring assembly or the encoder and, therefore, the situation was left as is. It should be noted that in the future, the shaft should be made out of a hardened steel since it is subject to much abuse during the construction process.

The bent shaft led to a slight off centered mass and, consequently, led to small vibrations in the filament winding machine. The dampers, which connected the mandrel to the frame, did not minimize the vibrations as expected and were replaced with steel blocks. The stiffness of the blocks allowed the vibrations of the mandrel to transition directly to the frame. The frame's stiffness performed an excellent job in restricting the vibrations and no significant vibrations were transferred to the oven which encompassed the machine. In addition to minimizing the vibrations, the frame maintained a secure platform during operations at various speeds and experienced no adverse effects to resonance frequencies.

The prepreg material cured at different rates when maintained at different temperatures and times as shown in Table 8.1 [Chern, Moon, Howell, 1992]. A temperature too low would prevent complete curing while a temperature too high would cause the material to cure too quickly. If the tape cured before one layer was overlaid by the next, bonding between the layers would not occur.

Table 8.1

PREPREG CURE TIME VS TEMPERATURE

Temperature	Time	Degree of Cure
177° C	60 min	97.0%
200° C	10 min	75.5%
210° C	10 min	86.5%
225° C	10 min	98.0%

To determine the operating envelope, the mandrel was positioned in the oven such that the heat lamp bank and its shields directed the heat flux onto the mandrel. The mandrel and its outside discs were adjusted to wrap a cylinder with a 7.6 cm length. With the lamp bank activated, an attempt was made to determine what steady state heat flux could be obtained from the heat lamp bank before the radiation oven reached its upper temperature limits. The shields, unfortunately, were designed to keep heat away from the surrounding motion control motors and this goal was obtained only by reflecting the heat back to the lamp bank. The critical temperature for the lamp bank was 400° C which is the temperature where the connecting wiring would melt. The upper temperature of the motion control motors was 50° C. By introducing approximately 20 kW to the lamp bank, the temperature of the mandrel surface receiving the heat flux stayed constant at 260° C.

To wind prepreg tape under these conditions and achieve proper curing, it was calculated that the mandrel would have to rotate at an angular velocity not to exceed 6 rpm. The disadvantage of this rotational speed is the time expended conducting a winding operation. The advantage was the fact that the thermocouple injection assemblies did not need an extremely fast injection speed.

The preliminary experiments with the system involved winding two to three layers of filament tape around the mandrel. This exposed a problem of

removing the filament wound cylinder from the mandrel after the graphite-epoxy mixture had cured due to the resin adhering to the steel cylinder. The winding area on the mandrel was layered with aluminum foil to remedy this problem.

To insure consistent operation of the thermocouple injection system, 30 V were supplied to the solenoids at the time of firing. This voltage enabled the solenoid rod to overcome the friction imposed by the spring loaded piston which subsequently pushed the thermocouple forward. Unfortunately, this voltage level was higher than the maximum level recommended by the manufacturer and led to a finite life span of the solenoid. Recommended solutions to this problem are as follows:

- 1) When activating the solenoid, disconnect power after the solenoid has retracted and the thermocouple has been injected.
- 2) Reduce friction between the solenoid rod and piston via a lubricant.
- 3) Reduce the stiffness of the spring which forces the piston onto the solenoid rod.
- 4) Acquire and install solenoids with higher electrical operating ranges.

The primary experiment involved wrapping and curing a prepreg tape with a width of 0.46 cm. The finished composite cylinder would have an axial length of 7.6 cm with 10-20 layers of tape. This meant the experiment would be a helical winding process where the mandrel would make 16.67 revolutions for every layer generated by the tape. Forced air convection was employed to

prevent the lamp bank from overheating from such an extensive operation. Duct was connected from the main blowers of the radiation oven system and directed between the lamp bank and the shields. Additional forced air was directed onto the two motors of the motion control system to maintain convective cooling. The area of the shield focusing radiation heat to the mandrel was lined with aluminum foil to increase reflective properties of the shield and direct more heat to the mandrel.

Originally a power intensity of 17.75 kW was assigned with a mandrel speed of 3 rev/min to obtain the minimal temperature levels on the filament needed for curing during the winding process.

The software program for the motion control system is identified in Appendix K where the mandrel revolves at 3 rev/min while the carriage assembly travels parallel to the mandrel axis at 1.5 cm/min, then reverses course and travels back covering a distance of 7.6 cm both ways.

During the winding operation, the two thermocouples were injected at different times to monitor the filament temperature at different layers in the prepreg tape. An excerpt from the recorded data is graphed and shown in Appendix L. It is obvious that a temperature increase occurs periodically. Although the temperature increase vs thermocouple position was not recorded, it can be concluded that it occurred when the thermocouple and the tape surrounding it was exposed directly to the lamp bank. This exposure occurs

once every revolution. The chart also shows the temperature range of the tape and demonstrates the ability of the process to maintain the prepreg tape above its minimum curing range.

The winding process for the primary experiment lasted 3 hours and resulted in fabrication of a composite cylinder of 27 layers. Pictures of the final product are in Appendix J. Throughout the experiment, the lamp bank intensity was increased incrementally until the maximum output of 23 kW was reached and a steady state heat transfer was maintained. Forced convective cooling of the lamp bank was instrumental in allowing output of this magnitude.

Once completed, the filament wound cylinder was removed from the mandrel. The aluminum foil separating the mandrel from the filament facilitated easy separation. Unfortunately, creases in the aluminum foil caused uneven curing to the inner layers and may have detracted from the strength of the product [Garala, 1987]. To minimize or eliminate this problem, future placement of foil should be executed with care and precision. A satisfactory alternative to aluminum foil (i.e. steel foil) which is stiffer and more resistant to folding may be substituted.

APPENDIX A

An equation of displacement as a function of force for the frame was developed. As described in Chapter 2, the filament winding machine can be represented in terms of an effective mass, effective spring, and an effective damper. The system is acted upon by an input load which is a combination of the weight of the mandrel and the force due to an eccentric load on the mandrel while it is in motion. Consequently, the following simplified mechanical model pictured in Figure A.1 was formulated.

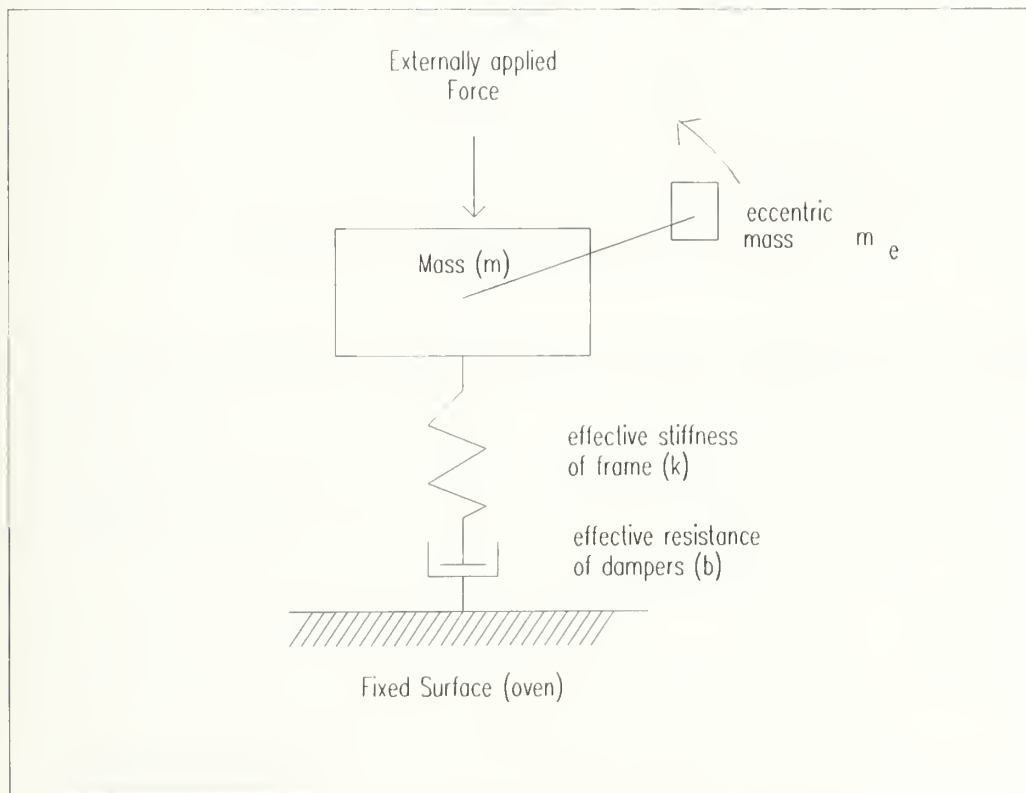


Figure A.1: Mechanical Representation of Machine

Next, the following bond graph model was developed from the mechanical model.

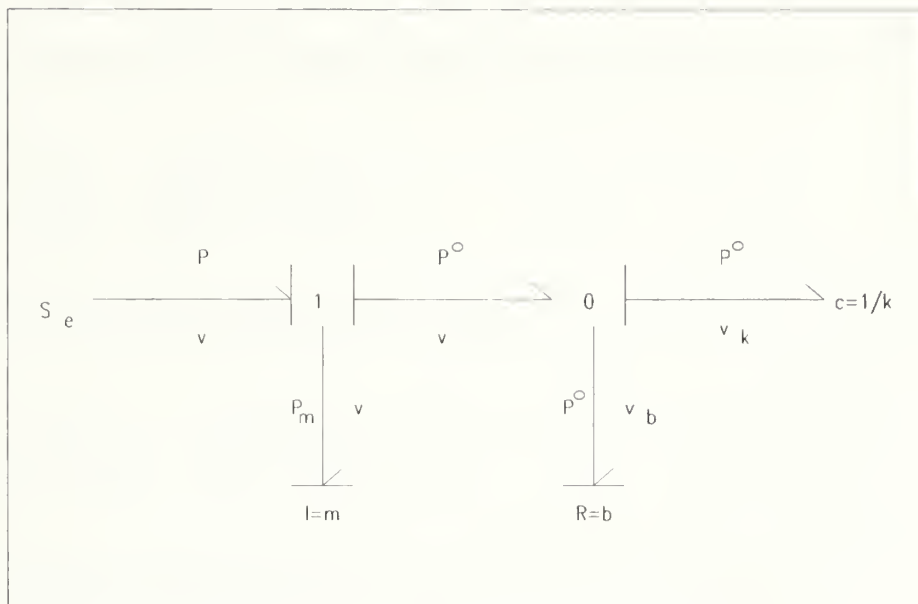


Figure A.2: Bond Graph Model of Machine

The following Constitutive and Junction equations were developed from the bond graph model.

Constitutive equations:

$$P_m = m \cdot v$$

$$P^\circ = b \cdot v_b$$

$$P^\circ = k \cdot x$$

Junction equations:

$$P = P_m + P^\circ$$

$$v = v_k + v_b$$

(A-1)

Since the independent energy storage elements are the mass and spring, p_m and x were chosen as the basic state variable to describe this system. The two first-order ordinary differential equations for this system can be written:

$$\frac{d}{dt} \begin{bmatrix} p_m \\ x \end{bmatrix} = \begin{bmatrix} 0 & -k \\ 1/m & -k/b \end{bmatrix} \cdot \begin{bmatrix} p_m \\ x \end{bmatrix} + \begin{bmatrix} 1 \\ 0 \end{bmatrix} P \quad (A-2)$$

Taking the derivative of equation (A-2) yielded:

$$\frac{d^2}{dt^2} \begin{bmatrix} p_m \\ x \end{bmatrix} = \frac{d}{dt} \begin{bmatrix} 0 & -k \\ 1/m & -k/b \end{bmatrix} \cdot \begin{bmatrix} p_m \\ x \end{bmatrix} + \frac{d}{dt} \begin{bmatrix} 1 \\ 0 \end{bmatrix} P \quad (A-3)$$

And extracting from equations (A-2) and (A-3):

$$\begin{aligned} \ddot{x} &= \frac{\dot{p}_m}{m} - \frac{k}{b} \dot{x} \\ \ddot{x} &= \frac{1}{m} (-kx + P) - \frac{k}{b} \dot{x} \end{aligned} \quad (A-4)$$

or

$$m \ddot{x} + \frac{km}{b} \dot{x} + kx = P$$

The standard form of equation (A-4) is:

$$\ddot{x} + 2\eta\omega_n \dot{x} + \omega_n^2 x = P(t) \quad (A-5)$$

$$\text{where } 2\eta\omega_n = \frac{k}{b}, \text{ or } \eta = \frac{\sqrt{km}}{2b}$$

and

$$\begin{aligned} \omega_n^2 &= \frac{k}{m} \\ P(t) &= \frac{P}{m} \end{aligned} \quad (A-6)$$

In the model, it was determined that the input load to the system is a combination of the static weight of the mandrel and the radial force due to the eccentric load of the mandrel in motion:

$$P = mg + m\omega^2 r \cdot \sin(\omega t) \quad (\text{A-7})$$

If the mandrel is at rest, the frame would deflect a specified amount due to the weight. The concern is not with this equilibrium position but with the deflection of the frame while the mandrel is under a constant rotational velocity. By neglecting the force due to the static weight and acceleration (change of frequency over time), the loads can be simplified to the following:

$$P = m_e \omega^2 r \cdot \sin(\omega t) \text{ and} \quad (\text{A-8})$$

$$P(t) = \frac{P}{m} = \frac{m_e \omega^2 r \cdot \sin(\omega t)}{m}$$

The result from equation (A-8) shows the implied load is a function of the eccentric mass to the total mass of the mandrel. Now assume a solution of x in the form of:

$$x = B \cdot \cos(\omega t) + C \cdot \sin(\omega t) \text{ or} \quad (\text{A-9})$$

$$x = B \cdot \sin(\omega t + \phi)$$

where angle ϕ is an out of phase response with respect to the input forcing function. Taking the first and second order differential equation of the assumed solution, yields:

$$\begin{aligned}\dot{x} &= \omega B \cdot \cos(\omega t + \phi) \\ \ddot{x} &= -\omega^2 B \cdot \sin(\omega t + \phi)\end{aligned}$$

(A-10)

then defining:

$$\begin{aligned}c &= \cos(\omega t + \phi) \\ s &= \sin(\omega t + \phi)\end{aligned}$$

Plugging (A-6), (A-7), and (A-8) into (A-5) obtained:

$$\begin{aligned}B(-\omega^2 s + 2\eta\omega_\eta\omega c + \omega_\eta^2 s) &= A \sin(\omega t) \text{ or} \\ B[(\omega_\eta^2 - \omega^2)s + 2\eta\omega_\eta\omega c] &= A \sin(\omega t) \\ \text{where } A &= \frac{m_e \omega^2 r}{m}\end{aligned}$$

(A-11)

The following are then defined:

$$\begin{aligned}\cos(\omega t + \phi) &= \cos(\omega t) \cos(\phi) - \sin(\omega t) \sin(\phi) \\ \sin(\omega t + \phi) &= \sin(\omega t) \cos(\phi) + \cos(\omega t) \sin(\phi) \\ \text{and} \\ \cos(\omega t) &\equiv c\omega t \\ \cos(\phi) &\equiv c\phi \\ \sin(\omega t) &\equiv s\omega t \\ \sin(\phi) &\equiv s\phi\end{aligned}$$

(A-12)

Plugging (A-12) into (A-11) yielded:

$$\beta[(\omega_\eta^2 - \omega^2)(c\omega t c\phi - s\omega t s\phi) - 2\eta\omega_\eta\omega(c\omega t c\phi + s\omega t s\phi)] = A s\omega t$$

(A-13)

By separating the above equation into two parts:

$$B[(\omega_{\eta}^2 - \omega^2)(s\omega t c\phi) - 2\eta\omega_{\eta}\omega(s\omega t s\phi)] = As\omega t$$

$$B[(\omega_{\eta}^2 - \omega^2)c\omega t s\phi + 2\eta\omega_{\eta}\omega c\omega t c\phi] = 0$$

or

$$[(\omega_{\eta}^2 - \omega^2)(c\phi) - 2\eta\omega_{\eta}\omega s\phi] = \frac{A}{B} \quad (A-14)$$

$$[(\omega_{\eta}^2 - \omega^2)s\phi + 2\eta\omega_{\eta}\omega c\phi] = 0$$

Solving for ϕ :

$$(\omega_{\eta}^2 + \omega^2)s\phi = 2\eta\omega_{\eta}\omega c\phi$$

$$\tan \phi = \frac{2\eta\omega_{\eta}\omega}{\omega_{\eta}^2 + \omega^2} = \frac{\sin \phi}{\cos \phi} \quad (A-15)$$

$$\phi = -\tan^{-1}\left[\frac{2\eta\omega_{\eta}\omega}{\omega_{\eta}^2 - \omega^2}\right]$$

$$= -\tan^{-1}\left[\frac{2\eta\varepsilon}{1 - \varepsilon^2}\right] \text{ where } \varepsilon = \frac{\omega}{\omega_n} \quad (A-16)$$

This solution is taken one step further by identifying the following:

$$\cos(\phi) = \frac{(1 - \varepsilon^2)}{d} \text{ and } \sin(\phi) = \frac{-2\eta\varepsilon}{d}$$

$$\text{where } d = \sqrt{(1 - \varepsilon^2)^2 + 4\eta^2\varepsilon^2} \quad (A-17)$$

Next, to find B by using (A-14):

$$\frac{(1 - \varepsilon^2)^2 + 4\eta\varepsilon \cdot \sin(\phi)}{d} = \frac{A}{B} \text{ or} \quad (A-18)$$

$$B = \frac{A}{d}$$

Plugging the values for B and ϕ into the assumed solution obtained the final solution of the forced response:

$$x = \frac{A}{\sqrt{(1 - \varepsilon^2)^2 + 4\eta^2\varepsilon^2}} \sin\left(\omega t - \tan^{-1}\left(\frac{2\eta\varepsilon}{1 - \varepsilon^2}\right)\right) \quad (\text{A-19})$$

APPENDIX B

To determine the thermal conduction properties of the mandrel, the radiative heat transfer of the oven to the filament was first determined. Once found, the heat loss from the mandrel to the wound composite was estimated. If the filament heat conduction through the mandrel to the surrounding medium was less than 5% of the total heat transfer from the heat source to the filament, then the model would be satisfactory. A two dimensional illustration of the heat source, filament and mandrel is shown in Figure B.1.

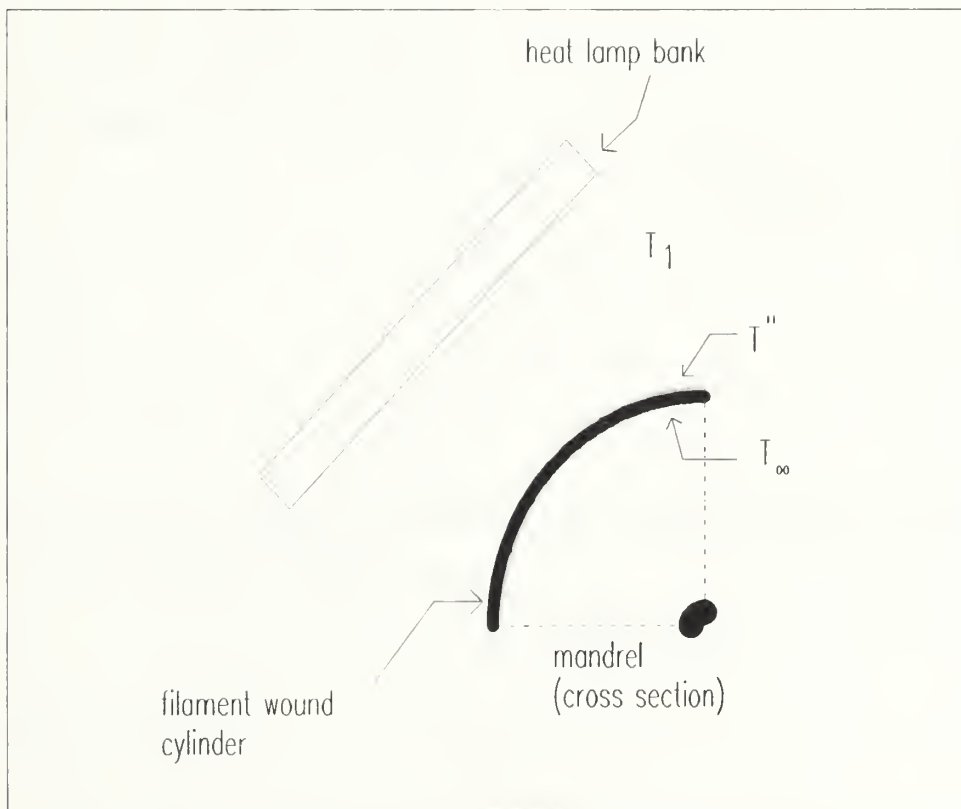


Figure B.1: Mandrel and Heat Lamp Bank

The radiation heat transfer to the filament wound cylinder is estimated [Edwards, Denny, Mills, 1979]:

$$q_{\text{rad}} = \sigma F_{14}^{\circ} \cdot \frac{(T_1^4 - (T'')^4)}{\frac{1 - \varepsilon_1}{\varepsilon_1 A_1} + \frac{1}{A_1 F_{14}^{\circ}} + \frac{1 - \varepsilon''}{\varepsilon'' A''}} \quad (\text{B-1})$$

Assigning the following values:

$$T_1 = 1000 \text{ K } (= 1340^{\circ}\text{F} = 1800^{\circ} \text{ R})$$

$$T'' = 350 \text{ K } (= 170^{\circ}\text{F} = 630^{\circ} \text{ R})$$

$$T_4 = 600 \text{ K } (= 621^{\circ}\text{F} = 1080^{\circ} \text{ R})$$

$$T_{\infty} = 294 \text{ K } (= 70^{\circ}\text{F} = 530^{\circ} \text{ R})$$

$$\varepsilon_1 = 1$$

$$A_1 = 0.4332 \text{ m}^2$$

$$F_{14}^{\circ} \cong 1$$

$$\varepsilon'' \cong .9$$

$$A'' = 0.254 \text{ m}^2$$

The total heat transfer by radiation from the heat lamp bank to the filament wound cylinder is estimated to be:

$$q_{\text{rad}} = 1.2 \text{ EE } 6 \text{ W}$$

Therefore, the heat loss through the mandrel should not exceed 5% or 61426 W.

A cut away view of the mandrel exposed from the front helped to develop the conductive heat loss equation.

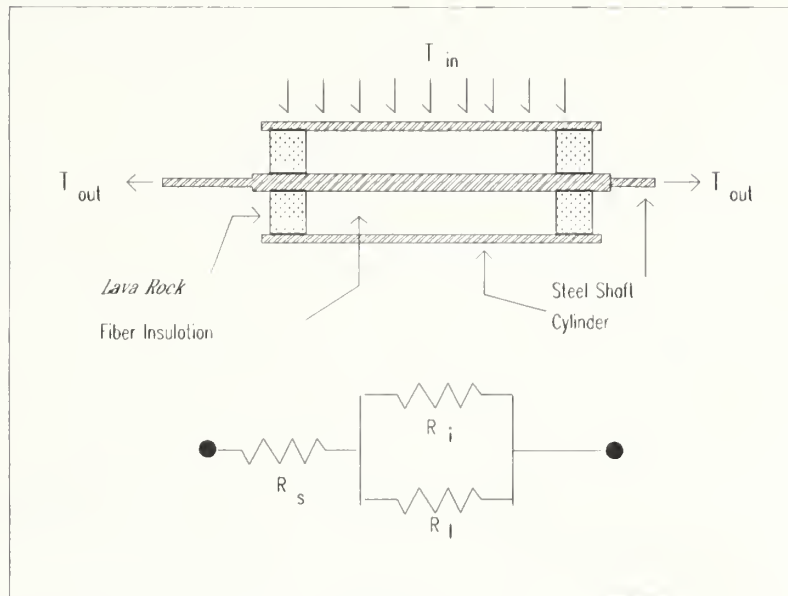


Figure B.2: Mandrel (Axial Section View)

To determine the conductive heat loss of the mandrel, the following assumptions are made:

- 1) The cylinder is infinitely long.
- 2) Conductive heat loss through the cylinder in the axial direction is insignificant.
- 3) The primary heat loss is radial.

$$q_{\text{cond}} = \frac{T_{\text{in}} - T_{\text{out}}}{R_{\text{tot}}}$$

where

$$R_{\text{tot}} = R_{\text{st}} + \left[\frac{R_l + R_i}{(R_l)(R_i)} \right] \quad (\text{B-2})$$

and

$$r_s = .013 \text{ m}$$

$$r_i = .0855 \text{ m}$$

$$r_o = .0887 \text{ m}$$

for steel;

$$L = 0.456 \text{ m}$$

$$k = 60.48 \frac{\text{J}}{\text{sec m } ^\circ \text{C}}$$

$$R_s = \frac{\ln \frac{r_o}{r_i}}{2\pi k L} \quad (3.4)$$

$$= 1.3 \text{ EE } - 5 \frac{\text{sec } ^\circ \text{C}}{\text{J}}$$

for the refractory material

$$L = .101$$

$$k_l = 7.8$$

$$R_l = 5.3 \text{ EE } - 3$$

and for the insulation

$$L = .355$$

$$k_i = 3.63$$

$$R_i = 3.3 \text{ EE } - 3$$

(B-3)

Therefore:

$$R_{\text{total}} = 5 \text{ EE} - 3$$

and estimating $\Delta T = 250^{\circ} \text{ C}$

$$q_{\text{cond}} = 43933 \frac{\text{J}}{\text{sec}} \text{ (W)} \quad (\text{B-4})$$

which is $< 61426.3 \text{ W}$, the maximum limit

APPENDIX C

To determine the exact dimensions of all the pieces of the mandrel, primary consideration was given to the difference in thermal expansion between the steel and refractory material. In order to maintain close tolerances between fitted parts, the initial design included press fitting the steel shaft and cylinder to the refractory material. Both materials would expand as the oven is heated, but the steel expansion would be more dramatic, resulting in a tensile azimuthal stress in the lava rock. It was essential to compute this tension to determine if it would stay within the design limits of the material. The following assumptions were made:

- 1) The stress state is essentially two dimensional in the radial and azimuthal directions (the axial direction is negligible).
- 2) No initial stress in either the mandrel nor the lava rock.
- 3) A uniform temperature increase over the thickness of the mandrel resulting in a uniform stress.
- 4) Start with no initial stress on the different parts of the mandrel, and uniform temperature increase.

For plane stress and thermal deformation [Shames, Cozzarelli, 1992]:

$$\begin{aligned}\varepsilon_x - \alpha\Delta T &= \frac{1}{E}(\sigma_x - \nu\sigma_y) \\ \varepsilon_y - \alpha\Delta T &= \frac{1}{E}(\sigma_y - \nu\sigma_x)\end{aligned}\tag{C-1}$$

with free expansion the radial deformation of a cylinder due to thermal effects will be [Lindeburg, 1984]:

$$\delta = r\alpha\Delta T \quad (C-2)$$

If the refractory material is press fitted onto the steel shaft, a pressure (p_r) is imposed externally on the shaft and internally on the lava rock. Consequently, both have resulting stresses and deformations. The equations in cylindrical coordinates which describe these stresses and deformations in the steel are [Ugural, Fenster, 1987]:

$$\begin{aligned} \sigma_{\theta s} &= -\frac{p_r r_{os}^2}{r_{os}^2 - r_{is}^2} \left(1 + \frac{r_{is}^2}{r^2} \right) \\ \sigma_{rs} &= -\frac{p_r r_{os}^2}{r_{os}^2 - r_{is}^2} \left(1 - \frac{r_{is}^2}{r^2} \right) \\ \delta_s &= -\frac{r_{os}^2 p_r r}{E_s (r_{os}^2 - r_{is}^2)} \left[(1 - \nu_s) + (1 + \nu_s) \frac{r_{is}^2}{r^2} \right] \end{aligned} \quad (C-3)$$

The stresses and expansion of the lava rock on its inner diameter is:

$$\begin{aligned} \sigma_{\theta l} &= \frac{r_{il}^2 p_r}{r_{ol}^2 - r_{il}^2} \left(1 + \frac{r_{ol}^2}{r^2} \right) \\ \theta_{rl} &= \frac{r_{il}^2 p_r}{r_{ol}^2 - r_{il}^2} \left(1 - \frac{r_{ol}^2}{r^2} \right) \\ \delta_l &= \frac{r_{il}^2 p_r r}{E_l (r_{ol}^2 - r_{il}^2)} \left[(1 - \nu_l) + (1 + \nu_l) \frac{r_{ol}^2}{r^2} \right] \end{aligned} \quad (C-4)$$

And the following is known [Ugural, Fenster, 1987]:

$$\delta_{\text{tot}} = \frac{r_{il}p_r}{E_l} \left(\frac{r_{il}^2 + r_{ol}^2}{r_{ol}^2 - r_{il}^2} + \nu_l \right) + \frac{r_{os}p_r}{E_s} \left(\frac{r_{is}^2 + r_{os}^2}{r_{os}^2 - r_{is}^2} - \nu_s \right) \quad (\text{C-5})$$

The dimensions for the shaft and lava rock for a press fit are listed below (properties of the steel shaft and the lava rock are listed in Table 1.1):

shaft

$$r_{os} = 1.27 \text{ cm}$$

$$r_{is} = 0 \text{ cm}$$

lava

$$r_{il} = 1.27 \text{ cm}$$

$$r_{ol} = 8.58 \text{ cm}$$

Additionally, the ΔT is estimated at approximately 260° C based on activation of the oven, and measuring the temperature of the mandrel at specified output parameters necessary to conduct experimental windings.

Combining the equations (C-2 through C-5) and inserting values determine that the radial expansion of the steel shaft is approximately 0.039 cm while that of the lava rock is approximately 0.0076 cm, with a net interference is 0.0314 cm. The resulting compressive pressure exerted internally on the lava rock and externally on the shaft is 2.8 EE7 Pa. Although the expansion is small, the resulting stress exceeds the design limits of the lava rock. Therefore a press fit, no matter how precise, is unsatisfactory and a gap must be designed into

the shaft/disc junction to allow for expansion. To achieve this gap, steel donuts were used and welded to the shaft. They were then bolted axially to the lava discs to allow a sufficient gap between the discs and shaft for thermal expansion. As the steel members expand due to thermal expansion, the bolts slide through slots made in the discs. These slots extend radially (Figure C.1). Additional steel donuts were bolted to the inside diameter of the cylinder and bolted axially to the discs. The discs were again slotted to allow for the cylinder to expand when heat inside the oven.

The mandrel was constructed with two disks affixed to the outside surface of the mandrel via a clamp assembly. These discs are designed to adjust axially along the cylinder and set the boundaries of the longitudinal boundary of the cylinder being wound. These discs are made of aluminum and lava rock. The aluminum and lava rock are affixed in the same manner as the donuts and lava rock inside the cylinder (Figure C.2). All slots in the refractory material were exaggerated to allow a factor of safety ranging from 2 to 10.

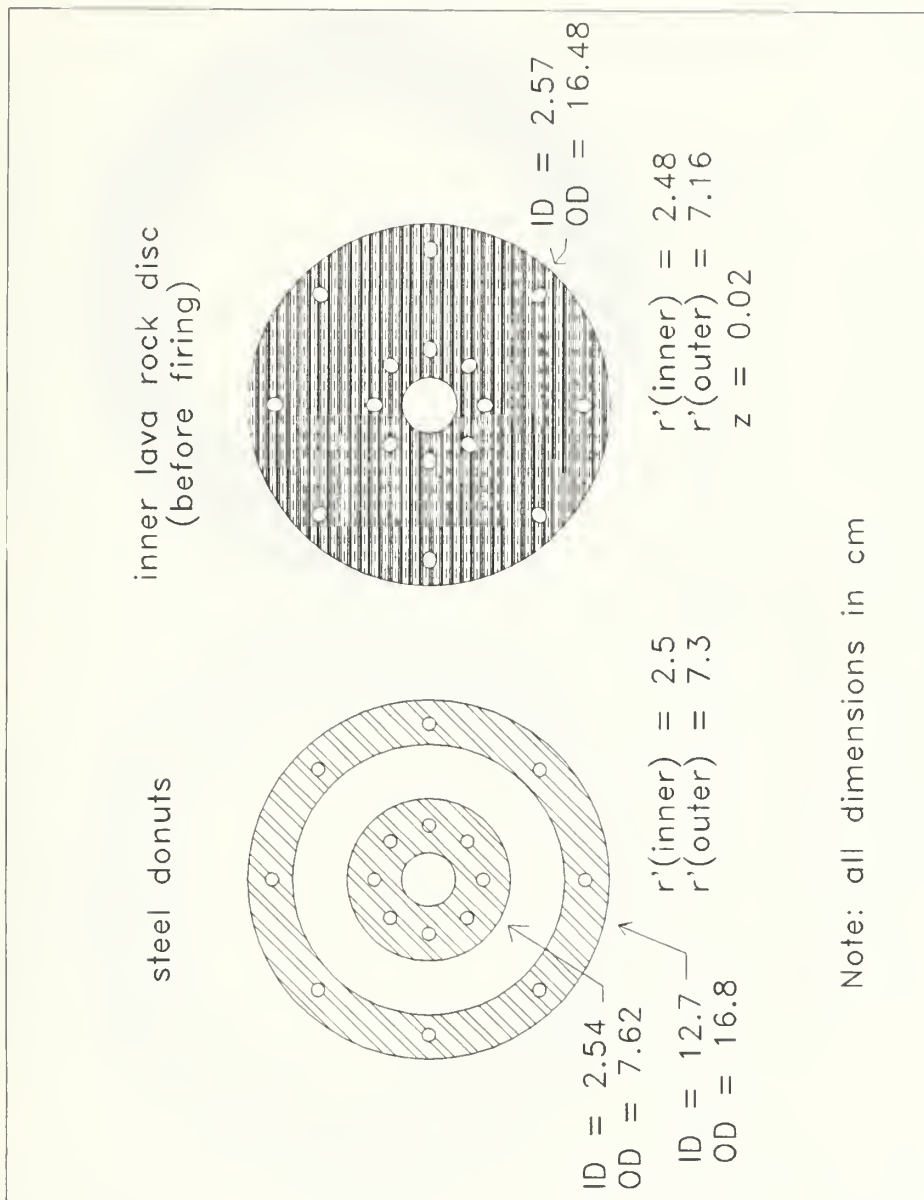
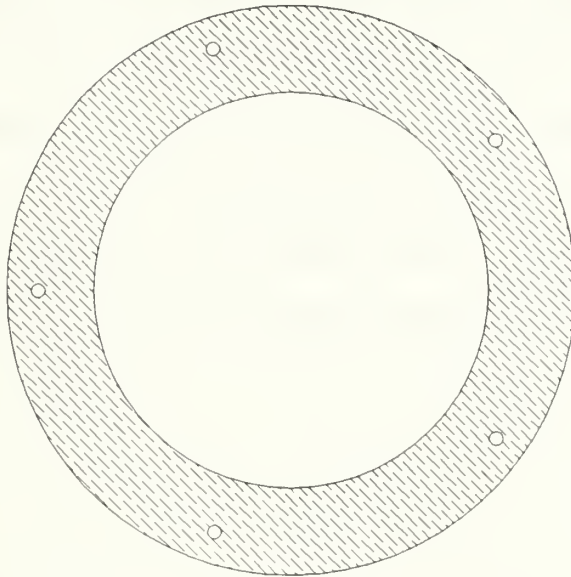


Figure C.1: Bolt Pattern (Inner Discs)

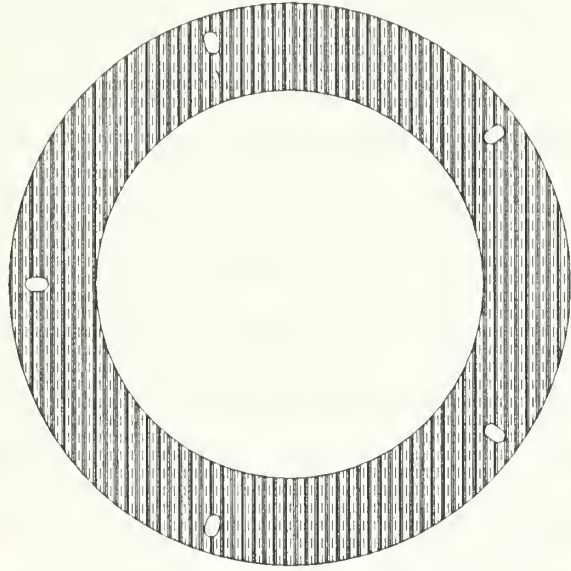
aluminum disc



ID = 17.8
OD = 25.65

$r' = 11.25$

outer lava rock disc



ID = 17.5
OD = 25.14

$r' = 11.2$
 $z = 0.36$

Note: all dimensions in cm

Figure C.2: Bolt Pattern (Outer Discs)

APPENDIX D

To determine potential prepreg tape slippage, consider a strand of filament with a width of 0.46 cm. Some slippage should be considered acceptable at the end of the mandrel where a change in winding direction may increase the axial force of the tow while it is being applied to the mandrel. It was decided that slippage equal to one quarter of the filament width is acceptable as shown in Figure D.1. The winding operation is helical, and the lateral placement of the composite is continuous (no gaps). One concern is the tow slippage at the end. It is at this area that the mandrel will rotate 180° while the tow transverses one quarter of its width in one direction and reverse course and travel the other direction the same distance as shown in Figure D.2. Figure D.2 also shows that the force due to friction must equal to or be greater than twice the tension in the axial direction. Slippage is not a problem if this condition is met. To determine the force due to friction, the vertical load on the mandrel exerted by the filament must be known. This load is statically equivalent to the normal pressure on the filament tape.

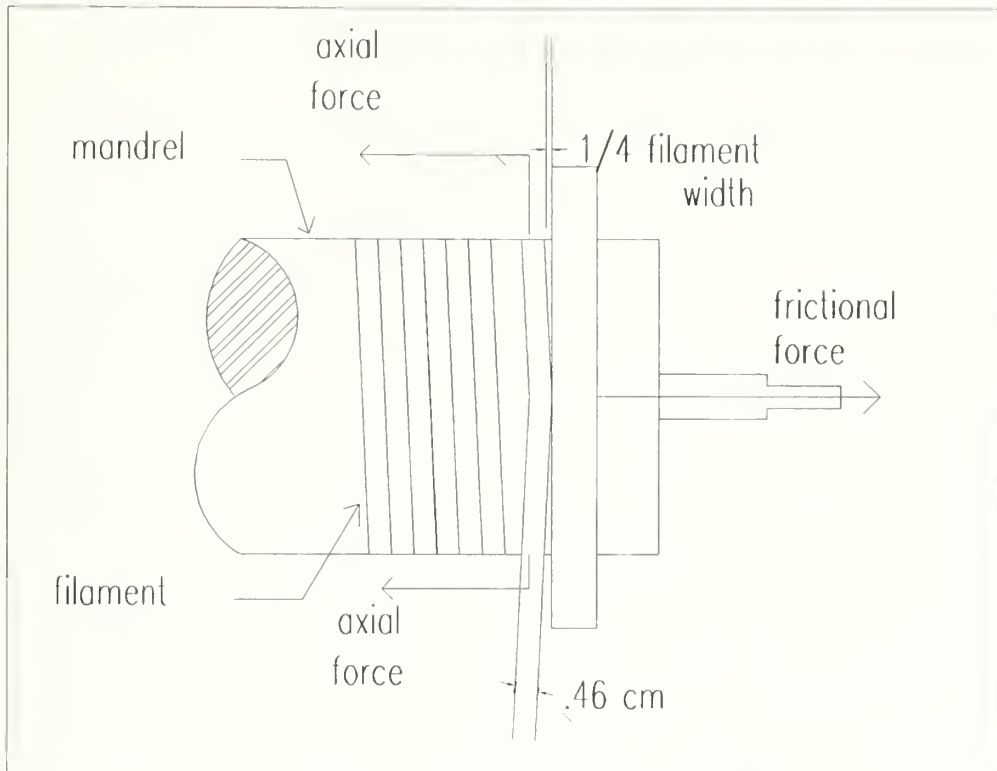


Figure D.1: Filament Wrapped Around the Mandrel

Since the tensioner is applying force at the source, it can be concluded that the filament already wrapped around the mandrel is applying 5 lbf (2.27 kg) in the opposite direction for equilibrium. This leaves a uniform 10 lbf (4.54 kg) exerted onto the mandrel and the mandrel exerts an equal amount in the opposite direction (radially) as shown in Figure D.2.

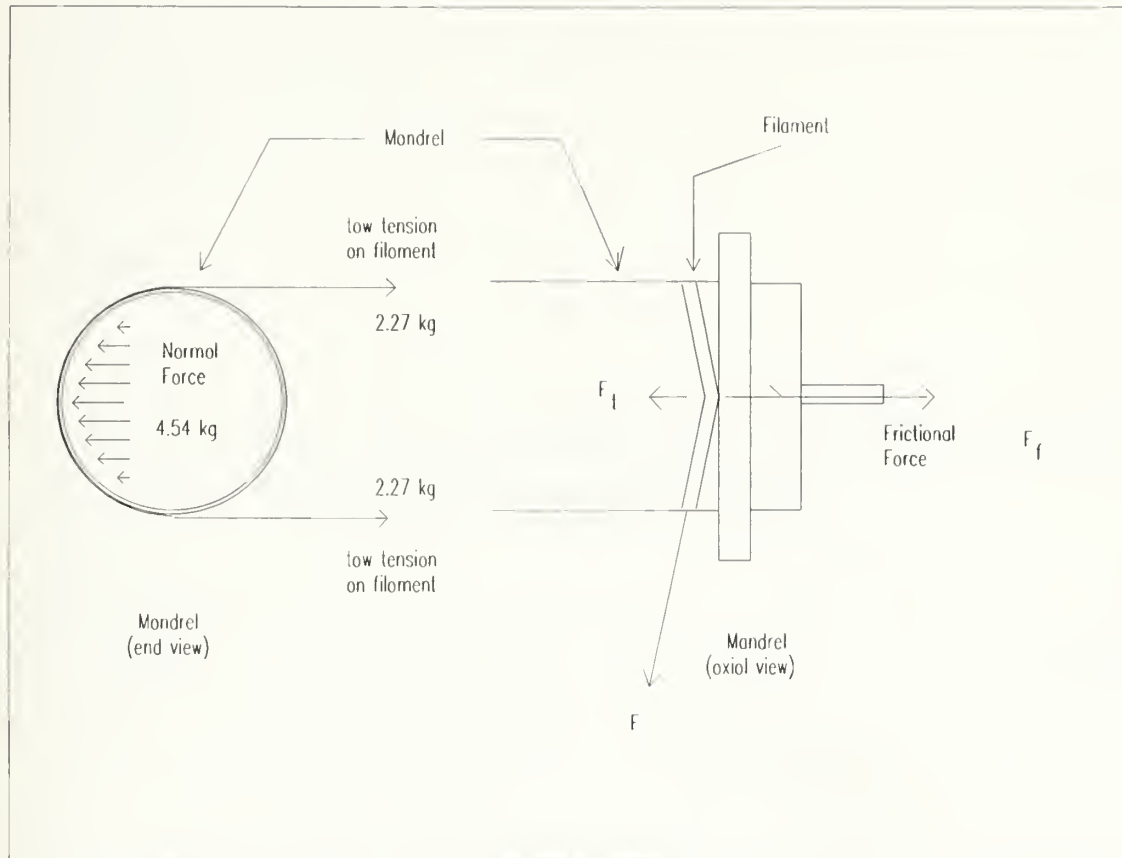


Figure D.2: Force Summation of the Filament

Knowing the angle of the filament with respect to the mandrel is about 0.5 degrees, the friction coefficient μ is determined and the maximum angle of the filament on the mandrel before unacceptable slippage occurs is calculated [Greenwood, 1988]:

$$\theta = 0.5^\circ$$

$$F = 2.27 \text{ kg}$$

$$N = 4.54 \text{ kg}$$

$$F_t = 2F \sin \theta$$

(D-1)

$$F_f = \mu N$$

$$\mu_{cs} = 0.25$$

$$\mu_{cc} = 0.16$$

It is evident that there will be less frictional force when the carbon is layered upon itself, thereby a better chance of slippage. Using μ_{cc}

$$2F \sin \theta_{\max} = \mu N$$

$$\theta_{\max} = \sin^{-1} \frac{\mu N}{2F}$$

(D-2)

$$\theta_{\max} = 9^\circ$$

Since the minimum angle for slippage is greater than the actual winding angle of 5 degrees, it can be concluded in the predicted helical winding pattern that slippage at the end of the mandrel will stay within satisfactory limits.

Of course, the maximum angle for slippage is still rather modest. Certain variables can be changed to reduce slippage when considering larger winding angles. For example, as the tow reaches the end of the mandrel during winding and must continue in the other direction, the axial displacement can be momentarily paused. This will allow application of the tow with no axial force and establish a larger normal force. One factor not yet considered is the frictional coefficient of the epoxy resin within the prepreg tape. Since the tape

is being thermally heated during the application, the epoxy is starting to bond and will therefore resist slippage.

APPENDIX E

The following three assumptions are made to analytically examine the stress on the lip:

- 1) The width of the lip is much longer than the thickness and the stress in the direction of the width are constant.
- 2) The tangential stress are negligible with respect to the radial stresses.
- 3) The load is uniform throughout the circumference of the lip and is constant throughout the thickness of the lip

Figure E.1 cuts and spreads out the lip so that it can be modeled as a cantilever beam of length 1.27 cm, width 56.06 cm, and depth 0.254 cm. Subsequently, the tangential and radial stresses in the original geometry become the normal stresses in the x and y direction respectively.

The deformation in the end of the beam will be 0.127 cm. Using Figure E.1 to determine if the load initiating this deflection will cause stresses exceeding the beam material's elastic limit and/or its ultimate tensile strength, the boundary conditions are set as follows:

$$\begin{aligned}\tau_{xy}\big|_{y=\pm g} &= 0 \\ \sigma_y\big|_{y=+g} &= -F \\ \sigma_y\big|_{y=-g} &= 0\end{aligned}\tag{E-1}$$

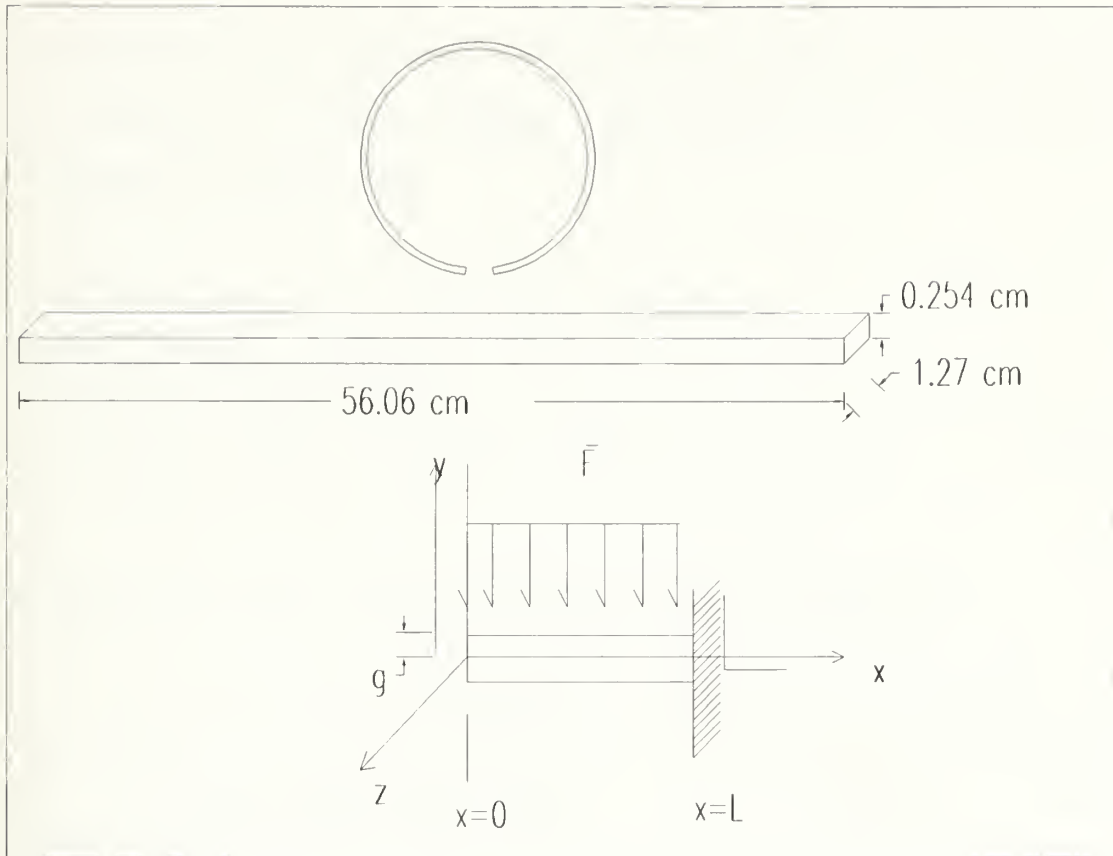


Figure E.1: Disc Lip

and at $x = L$:

$$\int_{-g}^{+g} \tau_{xy} dy = \bar{F} L$$

$$\int_{-g}^{+g} \sigma_x dy = 0$$

$$\int_{-g}^{+g} \sigma_x y dy = \frac{1}{2} \bar{F} L^2$$

and at $x = 0$:

$$\int_{-g}^{+g} \sigma_x y dy = 0$$

(E-2)

The intent is to solve the equation by considering a stress function in the form of a polynomial of the fifth degree. The solutions are in the form of [Timoshenko, Goodier, 1970]:

$$\begin{aligned}\sigma_x &= \frac{c_5}{3} x^3 + d_5 x^2 y - (2c_5 + 3a_5)xy^2 - \frac{1}{3}(b_5 + 2d_5)y^3 \\ \sigma_y &= a_5 x^3 + b_5 x^2 y + c_5 xy^2 + \frac{d_5}{3} y^3 \\ \tau_{xy} &= -\frac{1}{3} b_5 x^3 - c_5 x^2 y - d_5 xy^2 + \frac{1}{3}(2c_5 + 3a_5)y^3\end{aligned}\tag{E-3}$$

To solve for a_5, b_5, c_5, d_5 . making use of the boundary conditions:

$$\begin{aligned}\sigma_y|_{y=-g} &= 0 = a_5 x^3 - b_5 x^2 g + c_5 x g^2 - \frac{d_5}{3} g^3 \\ \sigma_y|_{y=g} &= -\bar{F} = a_5 x^3 + b_5 x^2 g + c_5 x g^2 + \frac{d_5}{3} g^3\end{aligned}\tag{E-4}$$

which leads to:

$$-\bar{F} = 2(a_5 x^3 + c_5 x g^2)\tag{E-5}$$

and at $x=L$

$$\frac{-\bar{F}}{2L} = a_5 L^2 + c_5 g^2\tag{E-6}$$

Next:

$$\begin{aligned}\tau_{xy}|_{y=g} &= 0 = \frac{1}{3}(2c_5 + 3a_5)g^3 \\ 0 &= \frac{1}{3}(2c_5 + 3a_5) \\ c_5 &= \frac{-3}{2} a_5\end{aligned}\tag{E-7}$$

With two equations and two unknowns the conclusion becomes:

$$a_5 = \frac{-\bar{F}}{(2L^2 - 3g^2)L}$$

$$c_5 = \frac{3\bar{F}}{2L(2L^2 - 3g^2)} \quad (E-8)$$

To find the next two variables, recall at $x=L$:

$$\begin{aligned} \int_{-g}^g \tau_{xy} dy &= \bar{F} L = -\frac{1}{3} b_5 x^3 y - \frac{1}{2} c_5 x^2 y^2 - \frac{1}{3} d_5 x y^3 + \frac{1}{12} (2c_5 + 3a_5) y^4 \\ &= -\frac{2}{3} b_5 L^3 g - \frac{1}{2} c_5 L^2 (0) - \frac{1}{3} d_5 L g^3 + \frac{1}{12} (2c_5 + 3a_5) (0) \\ -\frac{3}{2} \bar{F} &= b_5 L^2 g + d_5 g^3 \end{aligned} \quad (E-9)$$

and recall at $x=L$:

$$\begin{aligned} \int_{-g}^g \sigma_x y dy &= \frac{1}{2} \bar{F} L^2 = \int_{-g}^g \left[\frac{c_5}{3} x^3 y + d_5 x^2 y^2 - (2c_5 + 3a_5) x y^3 \right] dy \\ &= \frac{2}{3} d_5 L^2 g^3 - \frac{1}{15} (b_5 + 2d_5) g^5 \end{aligned} \quad (E-10)$$

Now combining the two summations listed below:

$$-\frac{3}{2} \bar{F} = b_5 L^2 g + d_5 g^3$$

$$d_5 = -\frac{b_5 L^2 g + 1.5 \bar{F}}{g^3} \quad (E-11)$$

With $L = 0.5''$ (1.27 cm) and $g = 0.05''$ (0.127 cm) results in the following:

$$\begin{aligned}
 \frac{1}{2}FL^2 &= -\frac{2}{3} \frac{\left(b_5 L^2 g + \frac{3}{2}F\right)}{g^3} L^2 g^3 - \frac{1}{15} \frac{\left(b_5 - 2b_5 L^2 g + 3F\right)}{g^3} g^5 \\
 &= -\frac{2b_5 L^4 g^4}{3g^3} - \frac{FL^2 g^3}{g^3} - \frac{b_5 g^5}{15} + \frac{2b_5 L^2 g^6}{g^3} - \frac{Fg^5}{5g^3} \\
 b_5 &= -F \frac{\left(\frac{3}{2}L^2 + \frac{1}{5}g^2\right)}{\left(\frac{2}{3}L^4 g + \frac{g^5}{15} + \frac{2L^2 g^3}{15}\right)} \\
 &= -(179.88)F \text{ [standard units]} \\
 &= -(11.06)F \text{ [SI]}
 \end{aligned} \tag{E-12}$$

and therefore:

$$\begin{aligned}
 d_5 &= \frac{(-179.88F)(L^2 g) + 1.5\bar{F}}{g^3} \\
 &= -(5987.84)\bar{F} \text{ [standard units]} \\
 &= -(368.3)\bar{F} \text{ [SI]}
 \end{aligned} \tag{E-13}$$

And from (E-8):

$$\begin{aligned}
 a_5 &= -4\bar{F} \text{ [standard units]} \\
 &= -0.246\bar{F} \text{ [SI]} \\
 c_5 &= 6.1\bar{F} \text{ [standard units]} \\
 &= -0.375\bar{F} \text{ [SI]}
 \end{aligned} \tag{E-14}$$

The final form of the original equations become:

$$\begin{aligned}
 \sigma_x &= \left[2.03x^3 - 5987.84x^2y - 0.2xy^2 + 4051.9y^3 \right] \bar{F} \quad [\text{standard units}] \\
 &= \left[0.125x^3 - 368.3x^2y - 0.012xy^2 + 249.2y^3 \right] \bar{F} \quad [\text{SI}] \\
 \sigma_y &= \left[-4x^3 - 179.88x^2y + 6.1xy^2 - 1995.95y^3 \right] \bar{F} \quad [\text{standard units}] \\
 &= \left[-0.246x^3 - 11.06x^2y + 0.375xy^2 - 122.8y^3 \right] \bar{F} \quad [\text{SI}] \\
 \tau_{xy} &= \left[59.96x^3 + 6.1x^2y + 5987.8xy^2 + 0.067y^3 \right] \bar{F} \quad [\text{standard units}] \\
 &= \left[3.7x^3 + 0.375x^2y + 368.3xy^2 + 0.004y^3 \right] \bar{F} \quad [\text{SI}]
 \end{aligned} \tag{E-15}$$

After computing the stress equations, the equation of displacement as a function of force is [Lindeburg, 1984]:

$$\begin{aligned}
 \delta &= \frac{\bar{F} L^4}{8EI_l} \\
 \text{where} & \\
 I_l &= \frac{Ld^3}{12} = 1.7 \text{ EE } - 3 \text{ cm}^4 \\
 E &= 6.9 \text{ EE } 10 \text{ Pa} = 6.9 \text{ EE } 6 \text{ N/cm}^2
 \end{aligned} \tag{E-16}$$

With a maximum deformation of 0.127 cm, the force/width exerted on the lip is 4581.2 N. Note this analysis is computing the force for a unit length along the lip. Plugging this value into (E-15) the stress becomes:

$$\begin{aligned}
 \sigma_x &= 2338.5 \text{ N/cm}^2 \\
 &= 2.3 \text{ EE } 7 \text{ Pa}
 \end{aligned} \tag{E-17}$$

Note the equation for deformation vs force was generalized only in the vertical direction. In reality there is a change in both the horizontal and vertical direction for a beam and the force is a function of both movements. This fact must be considered if a closer examination of the lip under loading is desired.

The yield stress of this material is approximately 3.1×10^{11} Pa. From these results it is obvious that the clamp will suffer minor permanent deformation due to the load needed to compress it. This is unimportant; the important issue is to insure the clamp will not fail. The applied loads do not exceed the ultimate stresses of the material, therefore failure is unlikely. In reviewing the endurance of the strength of the material it is discovered that aluminum does not have a well defined endurance limit. Since the yield stress of this material is well above the predicted load it must be assumed that the lip will have a infinite life expectancy.

APPENDIX F

Determining the potential deflection of the thermocouple was a straight forward problem when the thermocouple is treated as a cantilever Beam under a uniform load cause by its mass undergoing radial acceleration due to the spinning of the mandrel.

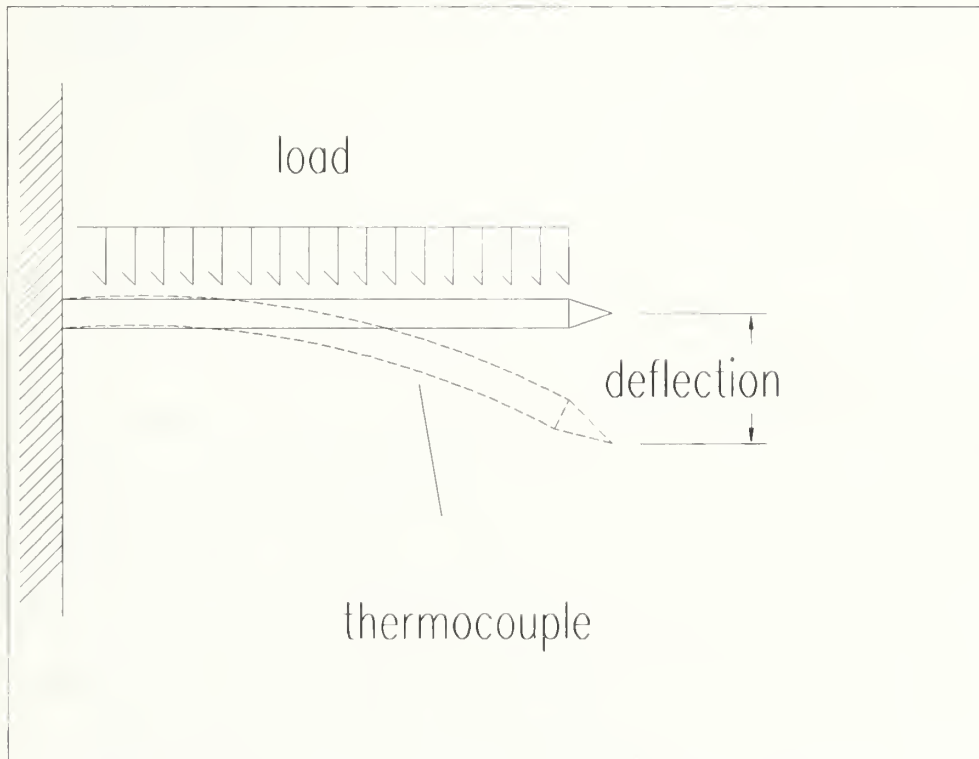


Figure F.1: Thermocouple under Centrifugal Force

The equation for this type of deflection is [Lindeburg, 1984]:

$$y_{\max} = \frac{wL^4}{8E_c I_x} \quad (F-1)$$

where:

$$d = 8 \text{ EE} - 4 \text{ m}$$

$$L = 5.08 \text{ EE} - 2 \text{ m}$$

$$m = \frac{\pi d^2 L \rho}{4} = 2.2 \text{ EE} - 6 \text{ (kN)}$$

$$a = \omega r_t = 14.13 \left(\frac{\text{m}}{\text{sec}^2} \right)$$

$$w \left(\frac{\text{force}}{\text{length}} \right) = \frac{ma}{L}$$

$$r_t = 0.098 \text{ m}$$

$$\rho = 87.3 \left(\frac{\text{kN}}{\text{m}^3} \right)$$

$$E_c = 119.0 \text{ GPa}$$

(F-2)

$$I_x = \frac{\pi d^4}{32}$$

The density value is that for copper since one of the two thermocouple wires is copper and the other wire is a material with material property values of the same magnitude as copper. Combining the values under the most severe conditions (when the rotational velocity is at its maximum of 720 rpm) it can be concluded that the thermocouple will deflect approximately $1.06 \text{ EE} - 7 \text{ m}$. This value is extremely small and is probably due to the high stiffness of the thermocouple relative to its mass.

APPENDIX G

The heat flow from the active lamp bank to the general outside area consists of radiation, conduction, and convection. The lamp bank emits radiation and creates a heat flux onto the mandrel and shields. The conduction is the heat flow through the steel shield to the ambient air inside the oven. Convection and radiation work in parallel to carry the heat to the outside air. In this particular case, it is assumed the heat flux at all points is constant in time when the environment reaches steady state, the radiation heat transfer inside the shield dominates the heat transfer, and the conductive resistance and radiation resistance outside the shield are extremely small.

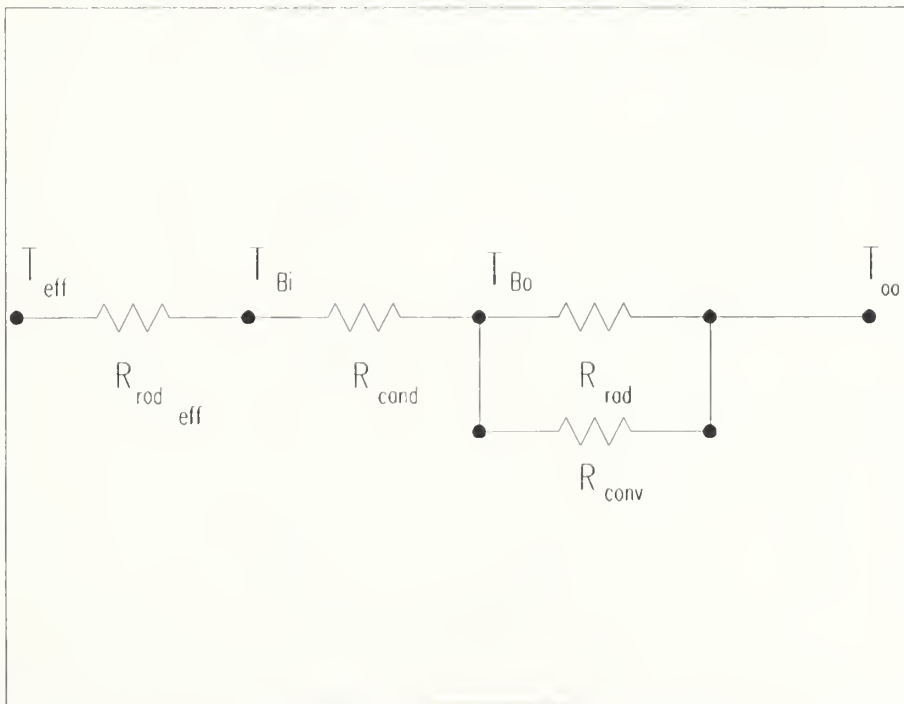


Figure G.1: Heat Transfer Network from the Lamp Bank to the Outside Air

The primary objective in developing this model was to find the net heat flux to the shields. A general two dimensional view factor for the radiation heat flux to the shielded area and mandrel must be determined by generalizing the shape of the lamp bank, shielded area, and mandrel as illustrated in Figure G.2, and assuming:

- 1) The lamp bank/mandrel combination is infinitely long.
- 2) The heat flow is constant along the axial length of the lamp bank.
- 3) All surfaces are gray and that emittance equals absorptivity.

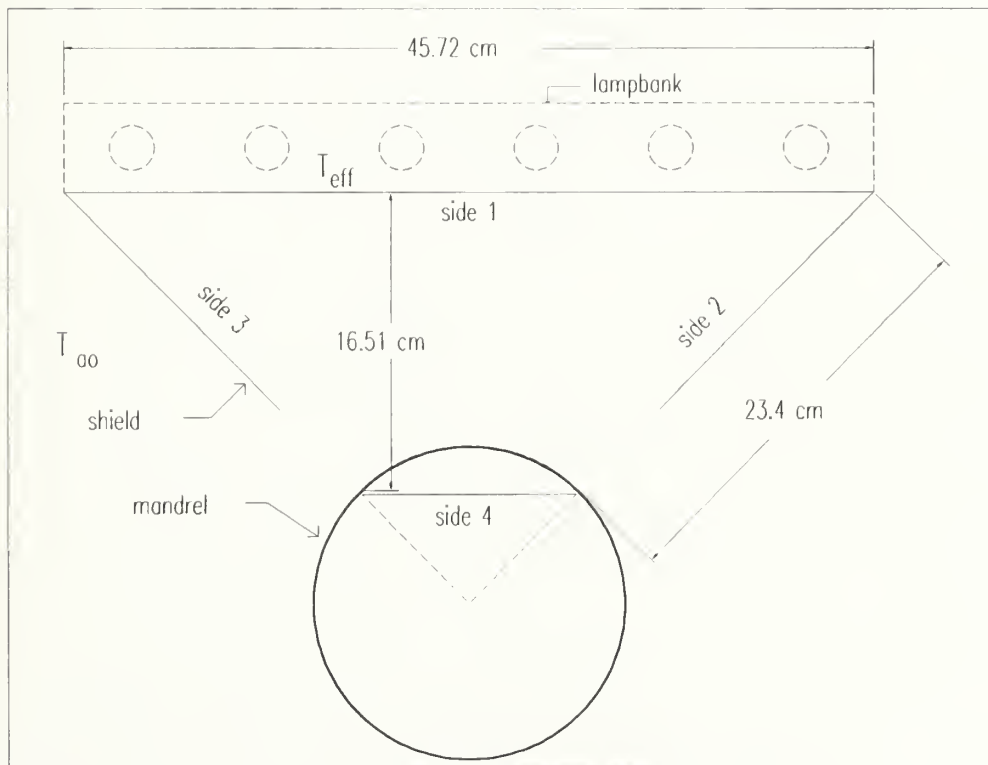


Figure G.2: Lamp Bank, Shields, and Mandrel Assembly

(End Section View)

The lamp bank is idealized as a uniform heat source (side 1) and the mandrel as a flat surface (side 4). The resulting geometry is an isosceles trapezoid as illustrated in Figure G.3.

This problem is conducted in two dimensions. The issue is the heat radiation on the shields which run along the entire length of the lamp bank. Knowing that the radiation heat transfer between the lamp bank, shields, and mandrel is governed by the simple enclosure analysis equations (G-1 and G-2) [Edwards, 1979]:

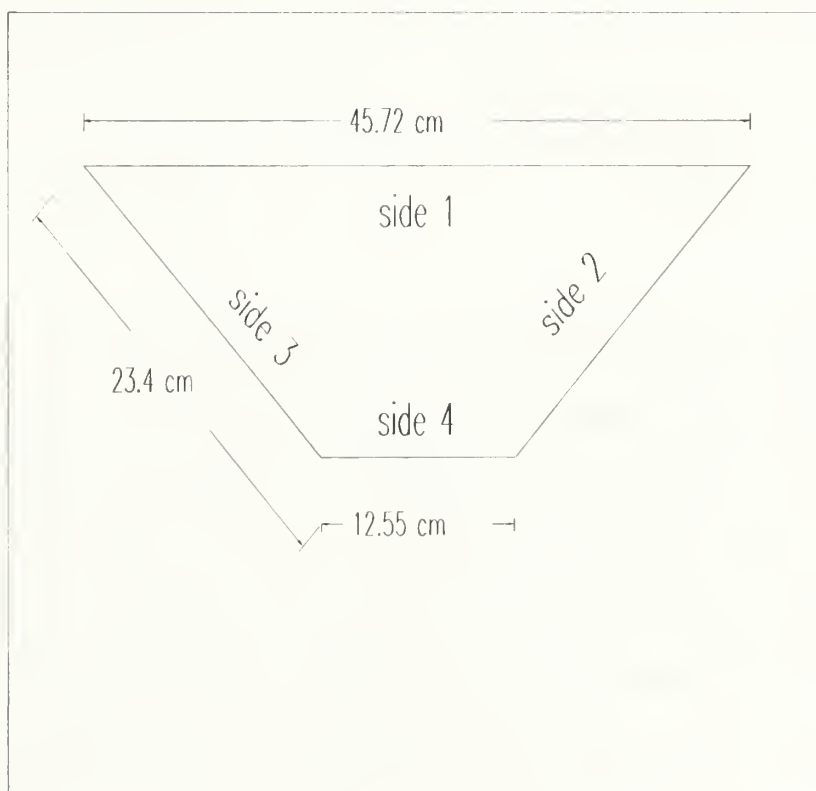


Figure G.3: Enclosure Geometry to Determine View Factor

$$A_i q_i^- = \sum_{j=1}^m q_j^+ A_j F_{j-i}$$

or through reciprocity

(G-1)

$$A_i q_i^- = \sum_{j=1}^m q_j^+ A_j F_{i-j}$$

or

$$q_i^- = \sum_{j=1}^m q_j^+ F_{i-j}$$

where

(G-2)

$$q_j^+ = \varepsilon_j \sigma T_j^4 + \rho_j q_j^-$$

Combining the last two equations, obtains:

$$q_i^- - \sum_{j=1}^m F_{i-j} \rho_j q_j^- = \sum_{j=1}^m F_{i-j} \varepsilon_j \sigma T_j^4$$

(G-3)

or

$$\sum_{j=1}^m (\delta_{ij} - F_{i-j} \rho_j) q_j^- = \sum_{j=1}^m F_{i-j} \varepsilon_j \sigma T_j^4$$

Equation (G-3) demonstrates that the radiation on each of the shields, the mandrel, and the lamp bank itself is a sum of the emitted and reflected heat fluxes on all the parts combined. For example, the incoming heat flux on the shield is the summation of the heat flux radiated by the lamp bank and that reflected by the other shield and the mandrel, minus the heat flux lost by the shield in question due to emissivity. Moreover, there is convection in this closed system but it is ignored under the assumption that radiation dominates inside the shielded area.

The ultimate intention is to find the total absorbed heat flux on either of the two sides of the shield. Values are now assigned to the different variables of the equation. By designing the shield (see Figure G.3), the shape factor is calculated on the different members. The view factor matrix is as follows:

$$F_{i-j} = \begin{bmatrix} 0 & .387 & .387 & .225 \\ .757 & 0 & .211 & .032 \\ .757 & .211 & 0 & .032 \\ .88 & .06 & .06 & 0 \end{bmatrix}$$

The sides of the shield will be layered with a foil having a very low absorptivity. Hopefully this foil will reflect much of the radiation inward and downward to the mandrel. Subsequently, the absorptivity and reflectivity matrix is as follows:

$$\alpha_i = \begin{bmatrix} 1 \\ .038 \\ .038 \\ 1 \end{bmatrix} \text{ and } \rho_i = \begin{bmatrix} 0 \\ .962 \\ .962 \\ 0 \end{bmatrix}$$

The low absorptance (emissivity) on the shields (sides two and three) results from the fact that a steel foil is placed inside the shield to reflect heat from the lamp bank away from the shield. A higher than expected temperature is estimated on the lamp banks in a hope to achieve the following temperature on the mandrel:

$$T_{\text{lampbank}} = 1000 \text{ K}$$

$$T_{\text{mandrel}} = 600 \text{ K}$$

But the lamp bank is made up of a series of individual lamps. Since it would be very cumbersome to include each lamp individually in the equation, an effective light emission location is identified and an effective light emission computed (Figure G.4).

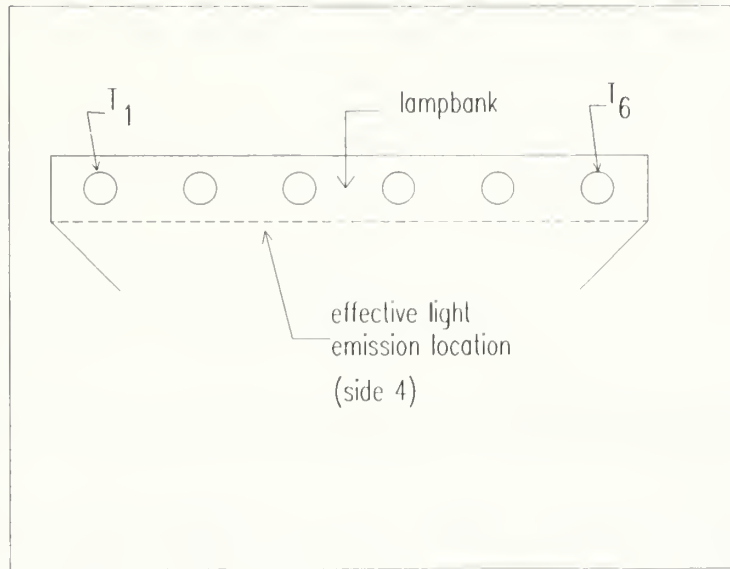


Figure G.4: Effective Light Emission on Lamp Bank

Defining the following radiation equations:

$$(\epsilon T^4)_{\text{total}} = \sum \epsilon_i T_i^4 \quad (\text{G-4})$$

and

$$(\epsilon T^4 A)_{\text{total}} = (\epsilon T^4)_{\text{eff}} \cdot A_a$$

or

$$(\epsilon T^4)_{\text{eff}} = \frac{(\epsilon T^4 A)_{\text{total}}}{A_a} \quad (\text{G-5})$$

And assigning values:

$$A_t = 2\pi r_t l_t n_t \text{ where}$$

$$r_t = 0.125" \text{ (0.32 cm)}$$

$$l_t = 38" \text{ (96.52 cm)}$$

$$n_t = 6 \text{ lights}$$

and

$$A_l = w_l \cdot l$$

for the "effective" lamp bank, compute:

$$(eT^4)_{\text{eff}} = 2.6 \times 10^{11} \quad (\text{G-6})$$

Consequently, for the mandrel, compute:

$$(\epsilon T^4)_4 = 1.3 \times 10^{11} \quad (\text{G-7})$$

The following matrix equation is obtained from the above formulas:

$$\begin{bmatrix} 1 & -0.372 & -0.372 & 0 \\ 0 & 1 & -0.203 & 0 \\ 0 & -0.203 & 1 & 0 \\ 0 & -0.058 & -0.058 & 1 \end{bmatrix} \begin{bmatrix} q_1^- \\ q_2^- \\ q_3^- \\ q_4^- \end{bmatrix} = \sigma \begin{bmatrix} 0 & 0.387 & 0.387 & 0.225 \\ 0.757 & 0 & 0.211 & 0.032 \\ 0.757 & 0.211 & 0 & 0.032 \\ 0.88 & 0.06 & 0.06 & 0 \end{bmatrix} \begin{bmatrix} 2.6 \times 10^{11} \\ \epsilon_2 T_2^4 \\ \epsilon_3 T_3^4 \\ 1.3 \times 10^{11} \end{bmatrix}$$

This matrix describes the heat transfer in the enclosure consisting of the lamp bank, shields, and mandrel. The heat transfer variables must be solved but there are now 4 equations and 6 unknowns. In analyzing the model, it is concluded that due to symmetry:

$$T_2 = T_3$$

$$q_2^- = q_3^-$$

These conditions reduce the system to 3 equations and 4 unknowns. In order to obtain one more equation, recall that the heat transfer from the source to the outside air is at steady state. Hence, it can be concluded that under steady state conditions with no heat absorption to the shields, the net incoming heat flux is equal to the convective and radiative heat flux exiting the shields to the outside air. An assumption is made that the temperature of the shields does not exceed a certain level and the heat flux exiting the shields is dominated by free convection. If valid, the absorbed heat flux will equal the emitted convective heat flux:

$$q_{2_{in}}^- = q_{2_{conv}}^+$$

To determine if this assumption is valid, the convective heat transfer coefficient is developed and inserted into equation (G-7):

$$q_{convection}^- = h_c (T_2 - T_\infty) \quad (G-8)$$

where

$$T_\infty \cong 294 \text{ K}$$

Next to find the value for the convective heat transfer coefficient, it is assumed natural convection with no condensation and a value for T_2 of 300 K.

For free convection in air at the assumed temperature [Edwards, 1979]:

$$h_c = \frac{N_u k_a}{L_i} \quad (5-13)$$

$$N_u = 0.332 \cdot \sqrt{Re} \cdot Pr^{.33}$$

$$Re^2 = \frac{\left(\frac{\Delta\rho}{\rho}\right)gL^3}{v_a^2} \quad (G-9)$$

$$Pr = .69$$

Next, values are found for the following convective variables:

$$L_i = \frac{\text{area}}{\text{perimeter}} = 5.35 \times 10^{-2} \text{ m}$$

$$k_a = 0.0267 \frac{\text{W}}{\text{m}^2\text{K}}$$

$$v_a = 50.6 \times 10^{-6} \frac{\text{m}^2}{\text{sec}}$$

$$g = 9.8 \frac{\text{m}}{\text{sec}^2}$$

$$\beta = \frac{1}{T_{\text{absolute}} (\text{K})}$$

$$\begin{aligned} \frac{\Delta\rho}{\rho} &\cong \beta(T_2 - T_{\infty}) \\ &= 2 \text{ EE } - 2 \end{aligned}$$

$$Re^2 = 11961.6 \quad (G-10)$$

$$N_{\mu} = 3.07$$

$$h_c = 1.53 \frac{\text{W}}{\text{m}^2\text{K}}$$

Subsequently, the convective heat transfer equation from the shield to the outside air becomes:

$$q_c^- = 1.53(T_2 - 294) \quad (G-11)$$

All 4 unknowns can be solved by combining (G-7 and G-11). Carrying out the calculations, it is found that the assumed value of T_2 is not valid. Additionally, it is found that forced convection will be necessary if natural convection cannot be relied upon to give a balanced equation without the shields becoming exceedingly hot. Recomputing the variables for air at 500 K, it is concluded that a steady state system can be maintained if a convective heat transfer coefficient of approximately $700 \text{ W/m}^2 \text{ K}$ is obtained. Unfortunately, this invalidates two earlier assumptions that convection inside the closed system is small when compared to radiation, and radiation outside the shields is small when compared to the convection. The original heat flux problem now becomes more difficult because radiation and convection must be considered both inside and outside the shields. The conclusion obtained thus far from the analysis is that forced convection is necessary on the shield to dissipate heat to restrain severe temperature increases on the shield.

APPENDIX H

To determine the view factor for the model, recall the defining geometry for a general three dimensional case. Figure H.1 identifies the defining geometry when discussing view factors. The general equation is defined by [Howell, 1982]:

$$dF_{d1-d2} = \frac{\cos a - \cos b}{\pi S^2} dA_2 \quad (H-1)$$

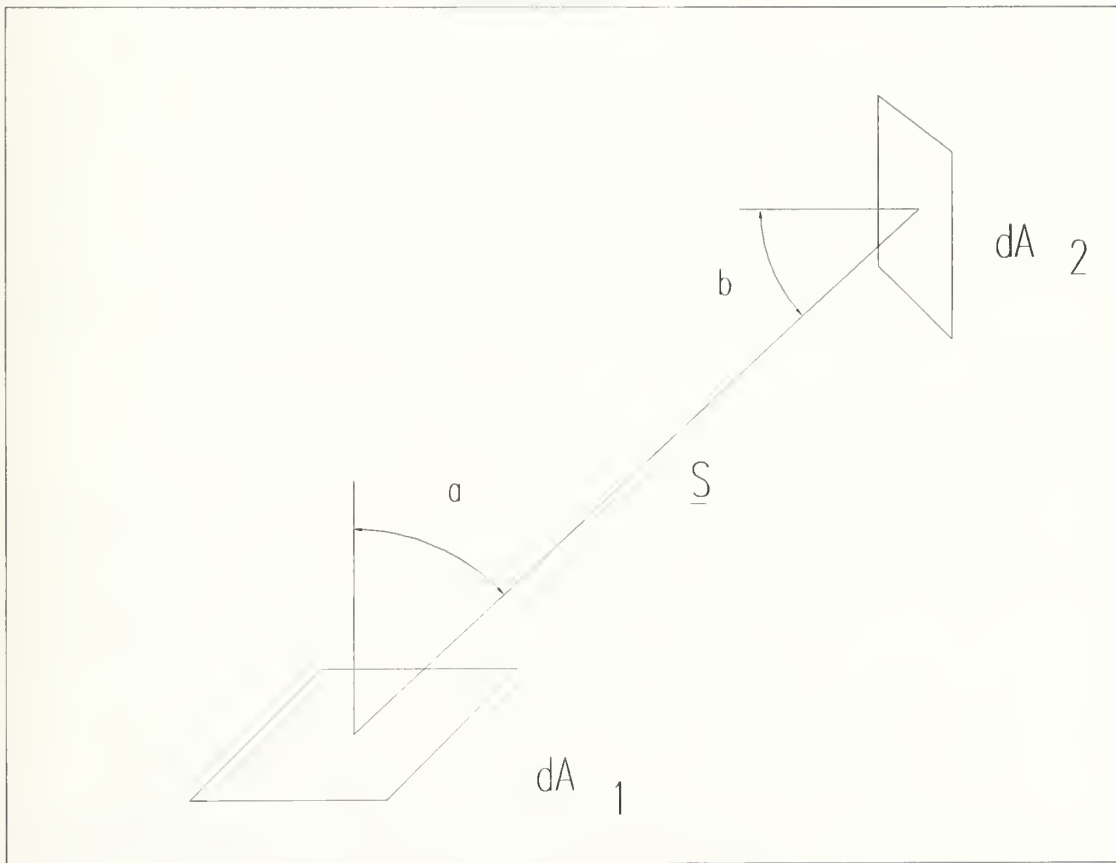


Figure H.1: Defining Geometry for View Factor

If the receiving element A_2 is a finite area, the configuration factor becomes:

$$\begin{aligned} F_{d1-2} &= \int_{A_2} \frac{\cos a \cdot \cos b}{\pi S^2} dA_2 \\ &= \int_{A_2} dF_{d1-d2} \end{aligned} \quad (H-2)$$

And, if both areas are finite, the equation becomes [Spindler, Gross, Hahne, 1981]:

$$F_{1-2} = \frac{1}{A_1} \int_{A_1} \int_{A_2} \frac{\cos a \cdot \cos b}{\pi S^2} dA_2 dA_1 \quad (H-3)$$

In this project, the goal is to focus a radiation source onto a section of the mandrel. The surface area of the radiation source is 813 cm^2 and the area of the mandrel which is exposed at any one time is approximately 97 cm^2 . The surface areas of both mandrel and lamp bank are bounded by shields

The apparent difference in size and orientation between the heat source surface and the exposed portion of the mandrel (which is generalized as a flat plate) is acknowledged from the onset. As a result, an efficient shape factor is not expected.

Fortunately, extensive work has been done previously by others to develop equations for varying shapes and configurations to determine the shape factor. One of these equations is used on the model. The most accurate equation is described below [Howell, 1982]:

Shape Factor of the mandrel to the lamp bank = F_{41}

$$= \frac{1}{(X_2 - X_1)(Y_2 - Y_1)} \sum_{l=1}^2 \sum_{k=1}^2 \sum_{j=1}^2 \sum_{i=1}^2 \left[(-1)^{i+j+k+l} G(A_{li}, B_{kj}) \right] \quad (\text{H-4})$$

where:

$$G(A_{li}, B_{kj}) = \frac{1}{2\pi} \left\{ \begin{aligned} & A_{li} \sqrt{1 + B_{kj}^2} \times \arctan \left(\frac{A_{li}}{\sqrt{1 + B_{kj}^2}} \right) \\ & - B_{kj} \times \arctan B_{kj} + \sqrt{1 + A_{li}^2} B_{kj} \arctan \left(\frac{B_{li}}{\sqrt{1 + A_{kj}^2}} \right) \\ & - \frac{1}{2} A_{li}^2 \ln A_{li}^2 + \frac{1}{2} \ln(1 + B_{kj}^2) - \frac{1}{2} \ln[1 + A_{li}^2 + B_{kj}^2] \end{aligned} \right\} \quad (\text{H-5})$$

and:

$$X = \frac{x}{z} \quad N = \frac{n}{z}$$

$$Y = \frac{y}{z} \quad S = \frac{e}{z}$$

$$A_{li} = S_l - X_i$$

$$B_{kj} = N_k - Y_j$$

The variables are graphically displayed in Figure H.2. Inserting these values yields:

$$F_{41} = 0.34 \quad (\text{H-6})$$

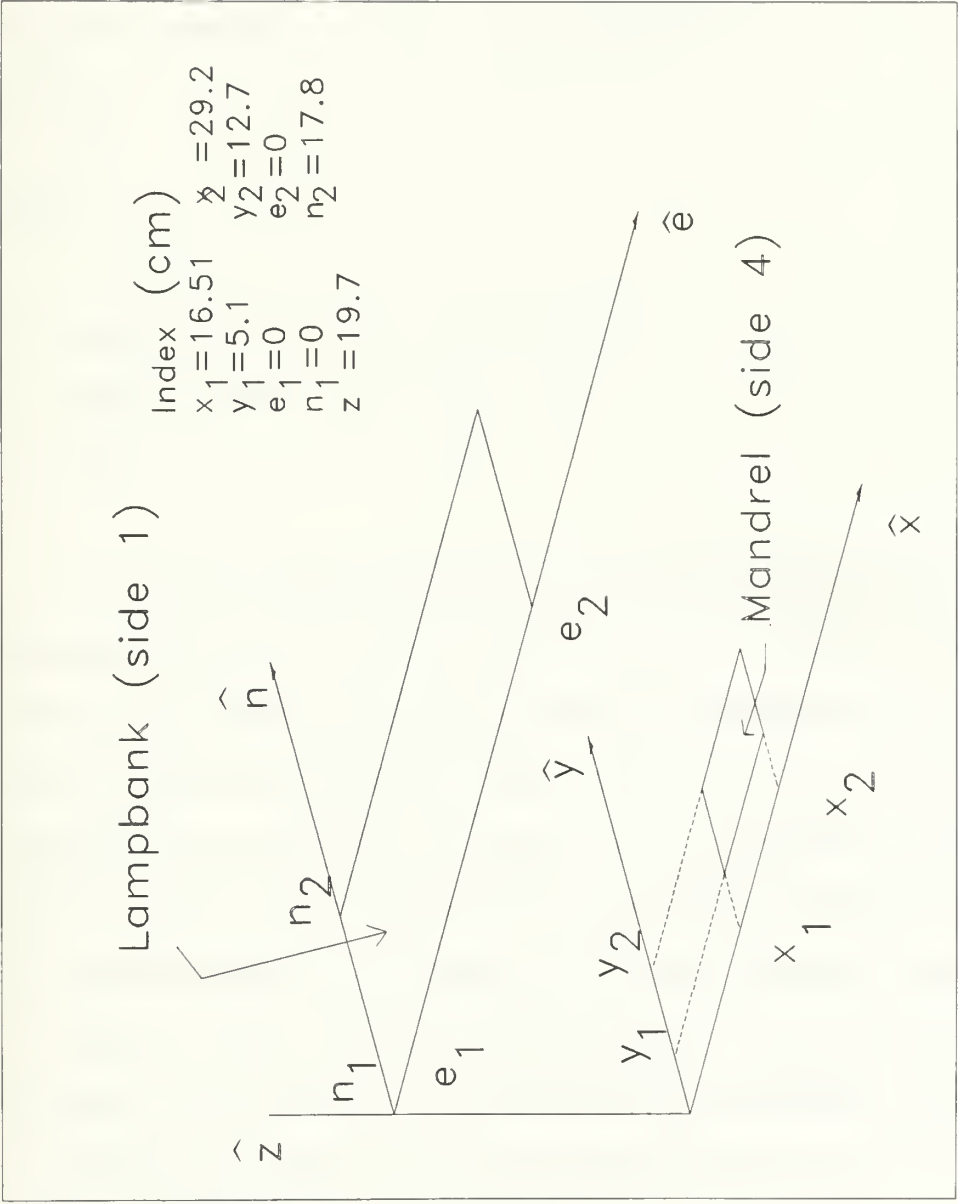


Figure H.2: Configuration of Mandrel to Heat Source

But this is the view factor of the mandrel to the heat source. The inverse is obtained by applying:

$$F_{14} = \frac{A_4}{A_1} F_{41} \quad (\text{H-7})$$

where:

$$A_4 = \text{exposed mandrel area} = 15\text{in}^2 \text{ (96.8 cm}^2\text{)}$$

$$A_1 = \text{heat source area} = 126\text{in}^2 \text{ (812.9 cm}^2\text{)}$$

$$F_{14} = 0.05$$

A software program designed to calculate the shape factor from an elemental surface to a finite area is used to check the validity of this equation [Alciatore, Lipp, 1989]. The program employs a hemisphere of unit radius to perform the Nusselt Geometric Analysis (Figure H.3). The 3-D Cartesian coordinate system originates at the center of the hemisphere. The origin also identifies the center of the elemental area. The surface with finite dimensions exists anywhere above the hemisphere. The Nusselt Geometric Analysis takes this surface of finite dimensions and transposes it onto the surface of the hemisphere. The shape factor is calculated from the transposed dimensions and the radius of the hemisphere. Note that the finite surface may not intersect nor exist below the hemisphere.

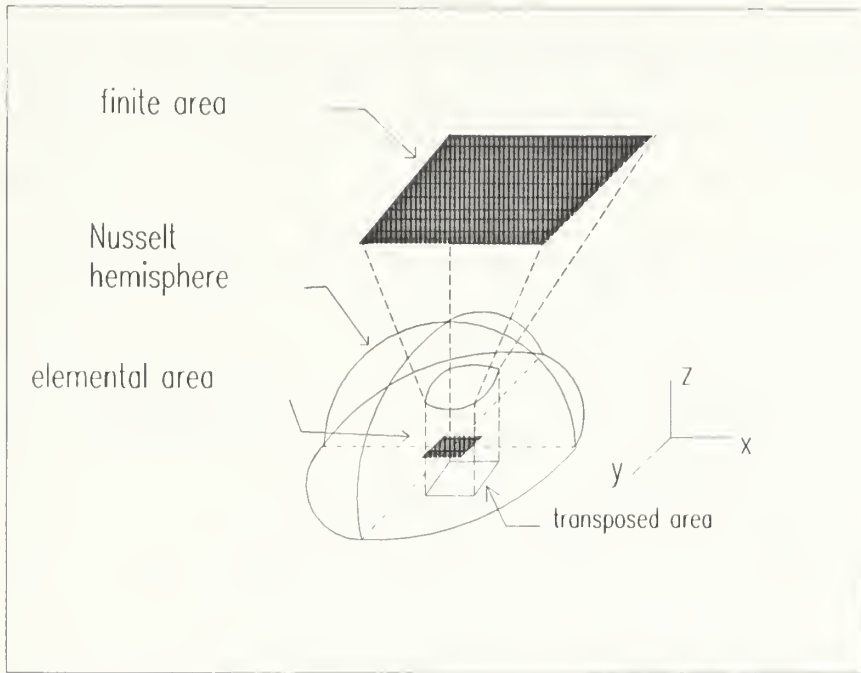


Figure H.3: Nusselt Geometric Analysis to Determine View Factor

To employ this software program, the radiation heat source is identified as a finite surface of specific dimensions and the exposed mandrel area as set of elemental areas approximately. By taking the view factor of each elemental area with respect to the finite surface area and adding the individual values, the view factor can be determined through the equation:

$$\sum_{dA} F_{S-dA} = F_{S-A}$$

using reciprocity:

$$\sum_{dA} \frac{dA \cdot F_{dA-S}}{A_s} = \frac{A}{A_s} F_{A-S} \text{ or}$$

$$\frac{1}{A} \sum F_{dA-S} = F_{A-S}$$

(H-8)

Note that both finite surface and elemental area can be divided along their respective lines of symmetry as shown below to reduce the size of areas to be treated.

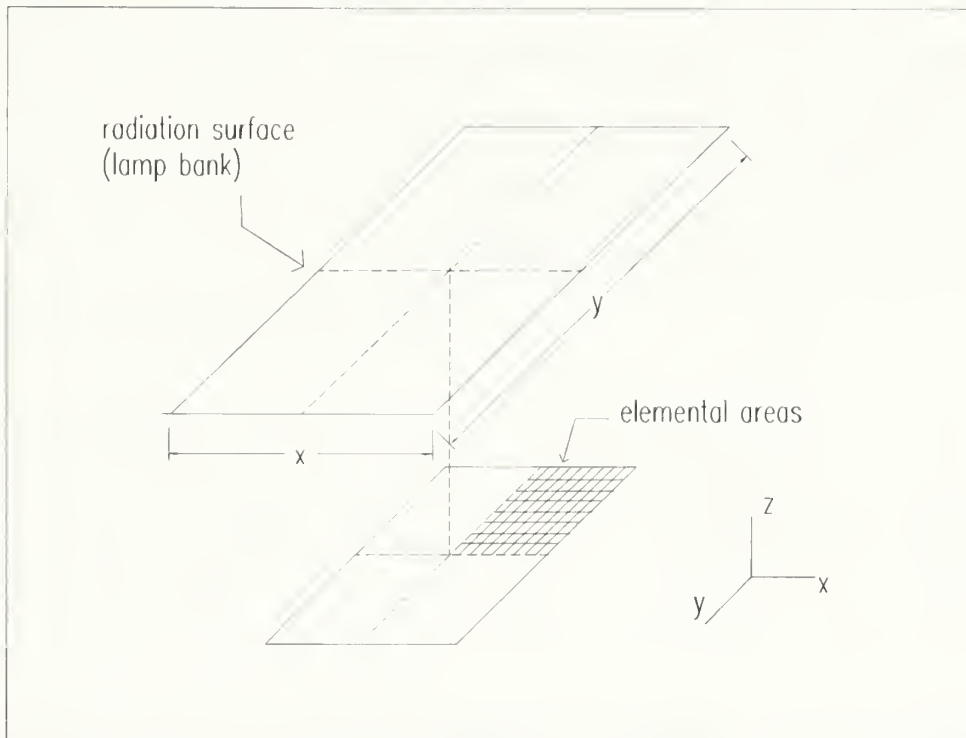


Figure H.4: Lamp Bank over Elemental Mandrel Area

This reduced the calculations by a factor of 4. Of course, the number obtained represents the view factor of the mandrel relative to the heat lamp surface, but this was easily reversed through the methods mentioned previously. The calculations resulted in a shape factor from the mandrel to the lamp bank of 0.3425 which closely matches the previous results. It can be concluded, therefore, both methods of determining the view factor were accurate.

APPENDIX I

The primary concern in sizing the motors for the motion control system was acceleration, constant velocity, and the time that the velocity could be maintained. The motor for the mandrel is identified as motor 1 and the carriage assembly motor as motor 2. The load for motor 1 consisted of the mandrel and the filament wound around it. The predetermined tension of the filament was between 1-5 lbf (4.5-22.5 N). With a maximum design speed of 720 rpm, the following was computed [Lindeburg, 1984]:

$$\begin{aligned}\omega &= 720 \text{ RPM} \\ d_m &= 17.8 \text{ cm} \\ v &= \omega \pi d_m = 670 \text{ cm/sec} \\ T_q &= t_f \cdot \frac{d_m}{2} = 2 \text{ Nm}\end{aligned}\tag{I-1}$$

It was anticipated that the time needed to accelerate would be roughly 13 seconds. Also, the motor to mandrel velocity would be a 2:1 ratio if motor 1 was connected to the mandrel via a belt assembly. The purpose of the belt was to allow flexibility in the positioning of the motor and absorb any unforeseen shock to the system in case of unexpected stoppage. The speed ratios were incorporated to allow a trade off of torque for speed. If the motor was allowed to turn faster than the mandrel, the acceleration torque could be reduced. These variables allowed the following:

$$\omega_{m1} = \omega \cdot 2 = 1440 \frac{\text{rev}}{\text{min}} = 24 \frac{\text{rev}}{\text{sec}}$$

$$\alpha_{m1} = \frac{\omega_{m1}}{t} = 1.84 \frac{\text{rev}}{\text{sec}^2} \quad (I-2)$$

The torque due to acceleration can be computed once the acceleration and mass moment of inertia of the mandrel are known. By dividing the mandrel into its components and measuring the dimensions and material characteristics of each part, the following are computed [Lindeburg, 1984]:

$$\begin{aligned} J_i &= \frac{\rho_i \pi l_i (r_o^2 - r_i^2)}{2} \\ J_s &= 0.833 \text{ lb in}^2 \left(2.4 \text{ kg cm}^2 \right) \\ J_{id} &= 59.52 \text{ lb in}^2 \left(174.33 \text{ kg cm}^2 \right) \\ J_{sc} &= 307.88 \text{ lb in}^2 \left(901 \text{ kg cm}^2 \right) \\ J_{isd} &= 13.62 \text{ lb in}^2 \left(39.9 \text{ kg cm}^2 \right) \\ J_{osd} &= 5.05 \text{ lb in}^2 \left(14.8 \text{ kg cm}^2 \right) \\ J_{od} &= 38.43 \text{ lb in}^2 \left(112.6 \text{ kg cm}^2 \right) \end{aligned} \quad (I-3)$$

Knowing:

$$g_c = 100.1 \frac{\text{cm kg}}{\text{sec}^2 \text{ N}} \quad (I-4)$$

$$T_{am1} = \frac{\alpha_m}{g_c} \sum J_i \quad (7.5)$$

$$= 0.23 \text{ Nm}$$

or

$$T_{m1} = 2.23 \text{ Nm}$$

The above torque is the minimum required with the known parameters. But a safety factor of two is added to make the required torque 4.5 Nm.

Torque computation of motor 2 is more difficult since it is connected to a screw driven rail table. The motor connects directly to the screw. The screw rotates and the pitch of the screw moves a coupling with one degree of freedom. The carriage is connected to the coupling and the screw pitch determines the distance the carriage will move per revolution. The design variables of this mechanism are:

$$v_c = 2.16 \frac{\text{in}}{\text{sec}} \left(5.5 \frac{\text{cm}}{\text{sec}} \right)$$

$$\omega_{m2} = 4.32 \frac{\text{rev}}{\text{sec}} = 27 \frac{\text{rad}}{\text{sec}}$$

$$w_c = 25 \text{ lb } (111.3 \text{ N})$$

$$\eta = 0.65$$

$$p_c = 2 \frac{\text{threads}}{\text{in}} \left(0.79 \frac{\text{threads}}{\text{cm}} \right)$$

$$R = 0.75 \text{ in } (1.9 \text{ cm})$$

$$L_s = 27 \text{ in } (68.6 \text{ cm})$$

$$\rho_s = 0.283 \frac{\text{lb}}{\text{in}^3} \left(7.8 \text{ EE } - 3 \frac{\text{kg}}{\text{cm}^3} \right)$$

As the carriage travels to one end of its path and initiates a return, a quick deceleration and acceleration must be programmed. The quicker this mechanism reaches speed, the sooner it will be in synchronous velocity with the

mandrel which will be operating at a constant velocity. Therefore, a time for acceleration is identified:

$$t = 0.05 \text{ sec}$$

The mass moment of inertia of various parts of the carriage assembly is computed:

$$\begin{aligned} J_{ls} &= \frac{\pi L \rho R^4}{2} = 3.4 \text{ lb in}^2 \quad (10 \text{ kg cm}^2) \\ J_c &= \frac{W}{(2\pi p)^2} = .158 \text{ lb in}^2 \quad (0.46 \text{ kg cm}^2) \\ J_{m2} &= 0.41 \text{ lb in}^2 \quad (1.2 \text{ kg cm}^2) \end{aligned} \tag{I-5}$$

Since the acceleration time for the carriage is extremely short, that the torque due to acceleration will be much greater than the torque at constant velocity.

This acceleration torque is computed as [Aerotech, 1988]:

$$\begin{aligned} T_{am2} &= \frac{1}{386} \left(\frac{J_c}{\eta} + J_{ls} + J_{m2} \right) \frac{w_c}{t} p_c \\ &= 1.7 \text{ in lb} \quad (0.19 \text{ Nm}) \end{aligned} \tag{I-6}$$

Again this torque was doubled when looking for a motor to meet the requirement for this project.

APPENDIX J

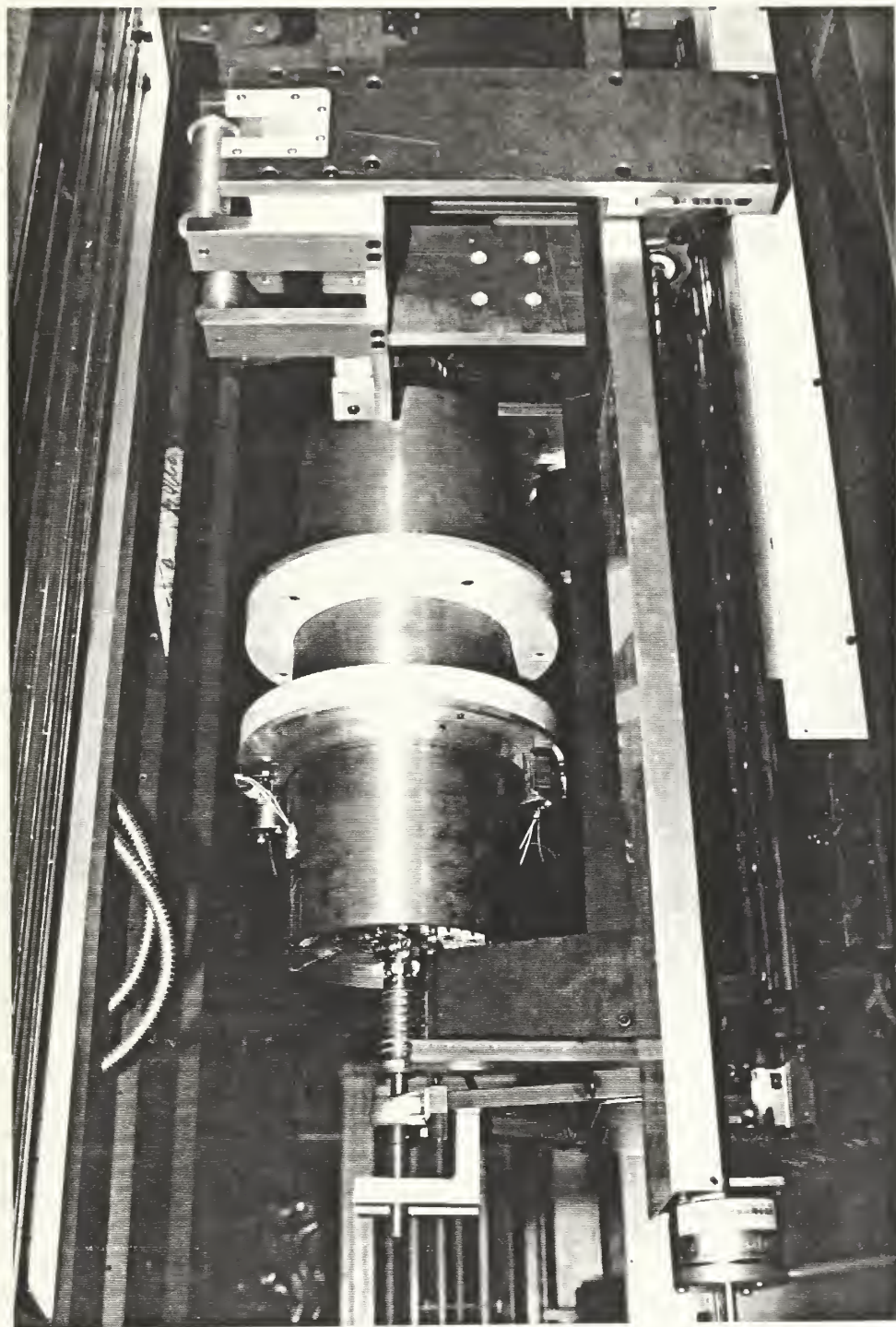


Figure J.1: Mandrel inside Oven

APPENDIX K

Listed below is the Software Program used in the primary filament winding experiment. The mandrel speed was set at 3 rev/min while the carriage speed was set at 1.5 cm/min. This program, if left unattended, would wrapped about 100 layers of graphite-epoxy tape around the mandrel. During the actual test, the program was terminated after 27 layers.

```
DEL PROG4    ; required to overwrite existing program PROG4
DEF PROG4
MA11
SCALE1
SCLA25000,25000
SCLV25000,25000
SCLD25000,25000
D15456000,45000
VAR1 = 1PM
VAR2 = 2PM
A2.0000,5.0000
AD0.2500,5.0000
V0.1665,0.0237
PSET0,0
MC10
COMEXC1
L
GO11
WAIT(2PM = 4.5)
IF(1PM < 1545.6 AND 2PM > = 4.5)
D,0
GO01
NIF
WAIT(2PM = 0.0)
IF(1PM < 1545.6 AND 2PM < = 0.0)
D,45000
NIF
IF(1PM > = 1545.6)
LX
NIF
LN
```


V0.0000,0.0000
GO11
COMEXCO
END

APPENDIX L

Figure L.1 displays the thermocouple-measured temperature of a small area of the filament on the mandrel over a period of time as the mandrel is rotating under an active lamp bank. This data was taken as the winding process was laying the second layer of tape onto the mandrel. The power input from the oven was 20 kW, the mandrel velocity was 3 rev/min and the tape width was 0.457 cm. The temperature increases are the result of the filament area passing under the direct radiation path of the lamp bank.

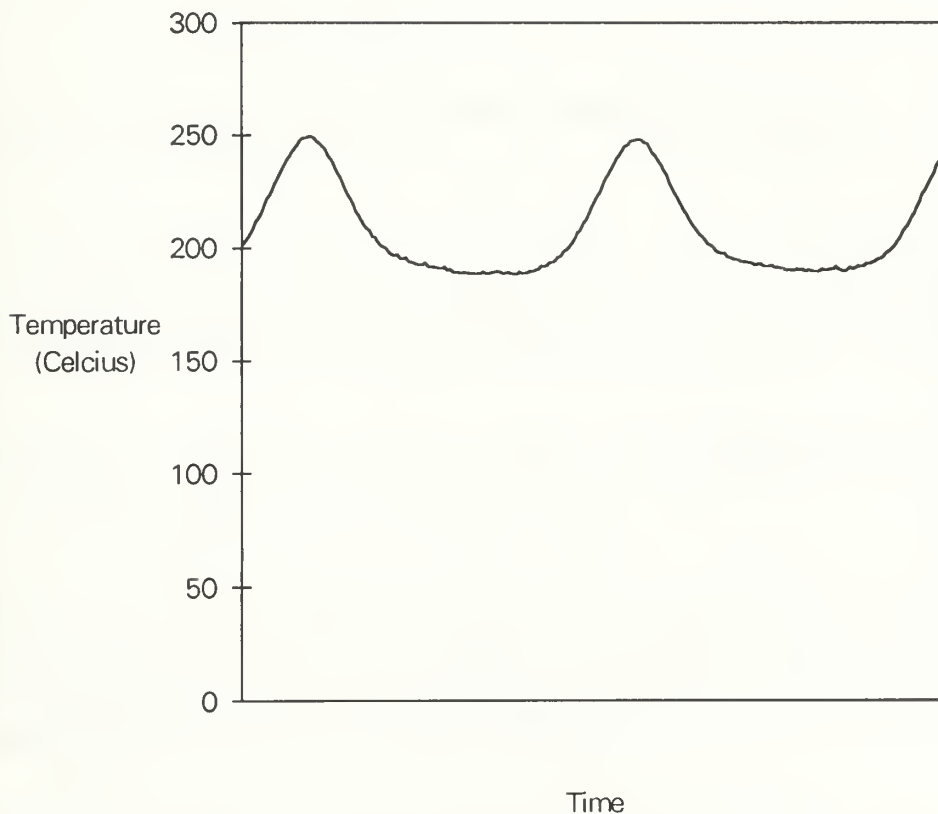


Figure L.1: Filament Temperature Profile over Time

REFERENCES

Aerotech Motion Control Product Guide, Aerotech, Incorporated, Pittsburg, PA, 1988, 107-109.

Alciatore, D. S., and W. S. Lipp, 1989. Closed Form Solution of the General Three Dimensional Radiation Configuration Factor Problem with Microcomputer Solution, Proc. 26th National Heat Transfer Conference, Philadelphia, PA, August 1989.

Bair, H. E., "Curing Behavior of an Epoxy Resin Above and Below T_g." Murray Hill, NJ: AT&T Bell Laboratories, n.d.

Bever, M., 1986. Encyclopedia of Material Science and Engineering, Oxford: Pergamon Press, 2578.

Chern, Bih-Cherng, T. J. Moon, and J. R. Howell, 1992. "Assessment of Using In-Situ IR-Heat to Cure Thermoset, Filament-Wound Structures," Proc. First International Conference on Transport Phenomena in Processing, 1303-1313.

Edwards, D. K., V. E. Denny, and A. F. Mills, 1979. Transfer Processes, 2nd ed. New York: McGraw-Hill, 141-147, 191-197.

Garala, H. J., 1987. "Experimental Evaluation of Graphite-Epoxy Composite Cylinders Subjected to External Hydrostatic Compressive Loading," Proc. 1987 Society for Experimental Mechanics Spring Conference on Experimental Mechanics, Houston, TX, June 1987, 948-951.

Ghosh, T. K., H. Peng, P. Banks-Lee, H. Hamouda, and D. H. Shin, 1991. "Analysis of Fabric Deformation in a Roll-Making Operation." Textile Research Journal, 61(4):185-192.

Greenwood, D. T., 1988. Principles of Dynamics, 2nd ed. New Jersey: Prentice-Hall, 114-115.

Hercules Product Data. Hercules, Incorporated, Wilmington, DE, n.d.

Howell, J. R., 1982. A Catalog of Radiation Configuration Factors, New York: McGraw-Hill, 5-10, 96-97.

Kaowool Ceramic Fiber Products. Thermal Ceramics, Incorporated, Augusta GA, April 1991.

Lindeburg, M. R., 1984. Mechanical Engineering Review Manual, 7th ed. San Carlos: Professional Publications, 14-1 - 14-24.

Loos, A. C., and G. S. Springer, 1983. "Curing of Epoxy Matrix Composites," Journal of Composite Materials, 17 (3):135-169.

Machinability Data Center, 1979. Machining Data Handbook, 2nd ed., Cincinnati: Metcut Research Associates, Inc., 729-57.

Maryland Lava. Maryland Lava Company, Incorporated, Bel Air, MD, n.d.

Omega, 1989. The Temperature Handbook, Omega Technologies Company, Stamford, CT, Chapter Z, 8-28.

Positioning Control Systems and Drives, Compumotor Digiplan, Rohnert Park, CA, n.d., Chapter A, 3-34.

Rohsenow, W. M. and J. P. Hartnett, 1973. Handbook of Heat Transfer, New York: McGraw-Hill, 15-30, 15-40.

Ryffel, H.H., R. E. Green, and J. H. Geronimo, 1989. Machinery's Handbook, 23rd ed. New York: Industrial Press, Inc., 512, 1286-1288.

Shames, I. H., and F. A. Cozzarelli, 1992. Elastic and Inelastic Stress Analysis, Englewood Cliffs, NJ: Prentice-Hall, 152.

Shigley, J. E., 1977. Mechanical Engineering Design, 3rd ed. New York: McGraw-Hill, 638-679.

Spindler, K., U. Gross, and E. Hahne, 1981. Letters in Heat and Mass Transfer, Vol 8, Pergamon Press Ltd, 219-227.

Timoshenko, S. P. and J. N. Goodier, 1970. Theory of Elasticity, 3rd ed. New York: McGraw-Hill, 35-39.

Ugural, A. C. and S. K. Fenster, 1987. Advanced Strength and Applied Elasticity, 2nd ed. Elsevier Science Publishing Co., Inc., 262-271.

Veeraraghavan, R., 1992. Operation and Design Improvement of a Prototype Experimental Filament Winding Machine, MFG 397 Project Report, The University of Texas at Austin, 10.

BIBLIOGRAPHY

Armaly, B. F., T. T. Lam, and A. L. Crosbie, 1973. "Emittance of Semi-Infinite Absorbing and Isotropically Scattering Medium with Refractive Index Greater than Unity," AIAA Journal (7):1498-1499.

Batra, S. K., D. S. Lee, and S. Backer, 1976. "On the Stress Analysis of Cylindrically Wound Packages: The Case of a Warp Beam," Textile Research Journal (6):453-459.

Rand, T., 1973. "Physical Properties of Newsprint Rolls During Winding," TAPPI 56 (6):153-156.

Yagoda, H. P., 1980. "Resolution of a Core Problem in Wound Rolls," Journal of Applied Mechanics 47 (12):847-853.

VITA

Mark Geoffry Lutkenhouse was born in Monterey, California on September 20, 1958, the son of Violet Newton Lutkenhouse and William Lutkenhouse. After completing his work at Bellamine College Preparatory School, San Jose, California, in 1976, he entered The University of California, Los Angeles. He received the degree of Bachelor of Science from The University of California, Los Angeles in August 1980. He was commissioned an officer in the United States Navy in October 1980 and became a pilot. He joined the United States Navy Civil Engineer Corps in 1986. In September, 1991, he entered The Graduate School at The University of Texas at Austin.

Permanent address: 986 Rosa Court

Sunnyvale, California 94086

This thesis was typed by the author.

DUDLEY KNOX LIBRARY
NAVAL POSTGRADUATE SCHOOL
MONTEREY CA 93943-5101



GAYLORD S



DUDLEY KNOX LIBRARY



3 2768 00018982 3